Atmos. Chem. Phys. Discuss., https://doi.org/10.5194/acp-2019-347
Manuscript under review for journal Atmos. Chem. Phys.
Discussion started: 13 May 2019
© Author(s) 2019. CC BY 4.0 License.

Atmospheric Chemistry and Physics Discussions

Global deposition of speciated atmospheric mercury to terrestrial surfaces: an overview

Lei Zhang[1,2,*], Peisheng Zhou[1], Shuzhen Cao[1], and Yu Zhao[1,2]

[1] School of the Environment, Nanjing University, 163 Xianlin Avenue, Nanjing, Jiangsu 210023, China

[2] State Key Laboratory of Pollution Control and Resource Reuse, Nanjing University, 163 Xianlin Avenue, Nanjing, Jiangsu 210023, China

Correspondence to: Lei Zhang (lzhang12@nju.edu.cn)

Abstract. One of the most important processes in the global mercury biogeochemical cycling is the deposition of atmospheric mercury, including gaseous elemental mercury (GEM), gaseous oxidized mercury (GOM), and particulate-bound mercury (PBM), to terrestrial surfaces. In this paper, methods for the observation of wet, dry, litterfall, throughfall, and cloud/fog deposition and models for mercury dry deposition are reviewed. Surrogate surface methods with cation exchange membranes are widely used for GOM dry deposition measurements, while observation methods for GEM dry deposition are more diverse. The methodology for Hg wet deposition is more mature, but the influence of cloud/fog scavenging is easy to neglect. Dry deposition models for speciated mercury have high uncertainties owing to the presence of sensitive parameters related to GOM chemical forms. Observation networks for mercury wet deposition have been developed worldwide, with the Global Mercury Observation System (GMOS) covering the northern hemisphere, the tropics, and the southern hemisphere. Wet deposition implies the spatial distribution of atmospheric mercury pollution, while GOM dry deposition depends highly on the elevation. Litterfall Hg deposition is crucial to forests. Urban areas have high wet deposition and PBM dry deposition because of high reactive mercury levels. Grasslands and forests have significant GOM and GEM dry deposition, respectively. Evergreen broadleaf forests bear high litterfall Hg deposition. Future research needs have been proposed based on the current knowledge of global mercury deposition to terrestrial surfaces.

Atmos. Chem. Phys. Discuss., https://doi.org/10.5194/acp-2019-347
Manuscript under review for journal Atmos. Chem. Phys.
Discussion started: 13 May 2019
© Author(s) 2019. CC BY 4.0 License.

Atmospheric Chemistry and Physics Discussions

1 Introduction

Mercury (Hg) is a global pollutant, characterized by its neurotoxicity, persistency and bioaccumulation effect. It undergoes regional or global long-range transport via atmospheric circulation, deposition to local or remote areas, methylation in ecosystems, and accumulation through food chain, posing high risks to human health and the environment (Obrist et al., 2018). Hg in the atmosphere has three major forms: gaseous elemental mercury (GEM), gaseous oxidized mercury (GOM), and particulate-bound mercury (PBM). The sum of the three Hg forms is named total mercury (TM). GOM and PBM are also known as reactive mercury (RM). GEM is the predominant form of atmospheric Hg (>90%) with a long residence time of several months to over one year due to its chemical inertness and low solubility. GOM accounts for less than 1% of atmospheric Hg, which is easily scavenged by wet deposition, resulting in a short residence time of hours to days. However, recent studies (Lyman et al., 2010; Gustin et al., 2013; McClure et al., 2014; Gustin et al., 2015) show that there could be a significant underestimation of GOM due to the low capture efficiency of the KCl denuder method adopted by most observation sites in the presence of ozone or moisture. PBM (<10% of atmospheric Hg) stays in the air for tens of hours to several weeks depending on particle size before scavenged by dry or wet deposition (Schroeder and Munthe, 1998; Lindberg et al., 2007; Ci et al., 2012; Fu et al., 2012; Zhang et al., 2016a).

Deposition is one of the most important processes in global Hg cycling, leading to the sink of atmospheric Hg (Obrist et al., 2018). Atmospheric Hg deposition can be broadly divided into wet and dry deposition. Hg wet deposition is associated with precipitation, cloud or fog, while Hg dry deposition is highly related to the underlying surfaces, including forest canopies, grasslands, wetlands, agricultural fields, deserts, background non-vegetated soils, contaminated sites, etc. (Zhang et al., 2009). Forest canopy is regarded as an important sink of atmospheric Hg for its special forms of deposition, litterfall and throughfall (Gustin et al., 2008). Litterfall is a form of indirect Hg dry deposition through foliar uptake of atmospheric Hg, and throughfall includes wet-deposited Hg above the canopy and a portion of dry-deposited Hg washed off from the canopy (Wright et al., 2016). Hg deposition through litterfall has recently been drawn much attention to by the study of Wang et al. (2016a). The sum of litterfall and throughfall represents the total Hg deposition on the forest canopy.

Atmos. Chem. Phys. Discuss., https://doi.org/10.5194/acp-2019-347
Manuscript under review for journal Atmos. Chem. Phys.
Discussion started: 13 May 2019
© Author(s) 2019. CC BY 4.0 License.

Atmospheric Chemistry and Physics Discussions

Significant efforts have been made in the past decade for quantifying atmospheric Hg deposition through both direct measurements and numerical models, especially on dry deposition (Lyman et al., 2009; Zhang et al., 2009; Holmes et al., 2011; Lai et al., 2011; Castro et al., 2012; Gustin et al., 2012; Peterson et al., 2012; Zhang et al., 2012; Fang et al., 2013; Sather et al., 2013; Lyman et al., 2014; Sather et al., 2014; Huang and Gustin, 2015a; Weiss-Penzias et al., 2016; Zhang et al., 2016b; Hall et al., 2017; Sprovieri et al., 2017). Yet large uncertainties still exist due to limitations of current methods for Hg deposition measurements and models (Gustin et al., 2015). The purpose of this paper is to give an overview of current understanding on the global deposition of speciated atmospheric Hg to terrestrial surfaces. In this paper, we reviewed methods adopted for Hg deposition measurements and modeling, results of Hg deposition observations from all over the world, and a summary of speciated atmospheric Hg deposition on different underlying surfaces.

2 Methods for Hg deposition measurements

2.1 Methods for Hg dry deposition

Three major categories of methods for direct Hg dry deposition measurements are the surrogate surface methods, the enclosure methods, and the micrometeorological methods (Zhang et al., 2009; Huang et al., 2014). Hg dry deposition can also be calculated based on Hg concentration measurements (Zhang et al., 2009; Wright and Zhang, 2015), which will be reviewed in Section 3.

2.1.1 Surrogate surface methods

Passive samplers are deployed in the surrogate surface methods to quantify the dry deposition flux of GEM, GOM and PBM (Huang et al., 2014; Wright et al., 2016). The Hg dry deposition flux is determined using the following equation:

$$F_{\mathrm{dry,SS}} = \frac{M}{A \cdot t} \quad (1)$$

where $F_{\mathrm{dry,SS}}$ is the Hg dry deposition flux using the surrogate surface methods, M is the total Hg amount collected on the material during the sampling period, A is the surface area of the collection material, and t is the exposure time.

Filter-based surfaces are widely used in passive samplers for Hg dry deposition flux measurements, with cation-exchange membrane (CEM) for GOM dry deposition (Lyman et al., 2007; Lyman et al., 2009; Castro et al., 2012; Huang et al., 2012; Peterson et al., 2012; Sather et al., 2012) and with gold-coated quartz fiber filter

© Author(s) 2019. CC BY 4.0 License.

(GcQFF) for TM dry deposition (Lai et al., 2011; Huang et al., 2012). The CEM method is believed to capture part of fine PBM as well (Huang et al., 2014). The CEM mounts for GOM dry deposition flux measurements are increasingly designed into aerodynamic shapes to minimize the impact of turbulence (Lyman et al., 2009). Water- or solution-based surfaces, e.g., static water surrogate surface (SWSS), collect GOM and PBM (Sakata and Marumoto, 2004; Marsik et al., 2007; Lai et al., 2011). GEM is not water soluble and hence unable to be captured by SWSS. Acidified solution captures part of GEM and has a higher measurement of Hg dry deposition than deionized (DI) water because in acidified solution GEM is oxidized to GOM which stabilizes the deposited Hg and decreases mass transfer resistance (Lai et al., 2011). SWSS was considered to measure TM dry deposition over ten years ago since RM (GOM and PBM) dry deposition was regarded as the dominance of TM dry deposition. In the recent decade, more and more studies found that GEM dry deposition accounts for a large proportion of TM dry deposition over grassland (Fritsche et al., 2008; Castro and Moore, 2016; Obrist et al., 2017). A newly developed artificial turf surrogate surface (ATSS) method has shown promising performance in measuring TM dry deposition and allows the interference of precipitation (Lynam et al., 2014; Hall et al., 2017). When Hg wet deposition is monitored simultaneously, the Hg dry deposition flux can be calculated as follows:

$$F_{\mathrm{dry,ATSS}} = \frac{(M_{\mathrm{turf}} + M_{\mathrm{throughfall}}) - M_{\mathrm{wet}}}{A \cdot t} \quad (2)$$

where $F_{\mathrm{dry,ATSS}}$ is the TM dry deposition flux estimated from the ATSS method, and M_{turf}, $M_{\mathrm{throughfall}}$ and M_{wet} are the Hg amounts in turf, throughfall and wet deposition, respectively.

Although surrogate surface methods have limitation in temporal resolution, they are still widely used in recent years due to their low costs, high accuracy and applicability to different Hg forms.

2.1.2 Enclosure methods

Enclosure methods rely on the conservation of mass and have been used for most GEM flux measurements due to their relatively low costs, portability, versatility and intuitive nature (Eckley et al., 2011; Sommar et al., 2013a; Sommar et al., 2013b; Agnan et al., 2016; Zhu et al., 2016; Ma et al., 2018). The dynamic flux chamber (DFC) method is the most commonly used enclosure method. A vacuum pump is

© Author(s) 2019. CC BY 4.0 License.

applied to draw air through a low Hg blank chamber at a constant flow, and the GEM concentrations at the inlet and outlet of the chamber are measured sequentially by a mercury analyzer coupled with a switchable valve. The GEM dry deposition flux is calculated according to the following equation:

$$F_{\mathrm{dry,DFC}} = \frac{Q(C_{\mathrm{inlet}} - C_{\mathrm{outlet}})}{A} \quad (3)$$

where $F_{\mathrm{dry,DFC}}$ is the GEM dry deposition flux measured by the DFC method, Q is the flushing flow rate, C_{inlet} and C_{outlet} are the GEM concentrations at the chamber inlet and outlet, respectively, and A is the area of the chamber footprint.

Different flushing flow rates, chamber designs and materials, as well as the lack of standard operating protocol and blank correcting procedures, make it hard for comparison between different studies (Eckley et al., 2010; Agnan et al., 2016; Osterwalder et al., 2018). A novel aero-DFC was designed and utilized in recent studies (Lin et al., 2012; Zhu et al., 2015a; Zhu et al., 2015b; Osterwalder et al., 2018). The GEM dry deposition flux under atmospheric condition can be calculated based on the flux measured by the aero-DFC with the internal shear property precisely controlled and the surface shear property (Lin et al., 2012).

Enclosure methods have high temporal and spatial resolution, and are thus widely adopted for GEM dry deposition flux measurements. However, they are not applicable to RM dry deposition measurements.

2.1.3 Micrometeorological methods

Micrometeorological methods can be mainly divided into the direct flux measurement methods and the gradient methods. The most known one of the former is the relaxed eddy accumulation (REA) method, while the latter include the aerodynamic (AER) method and the modified Bowen-ratio (MBR) method (Zhang et al., 2009; Yu et al., 2018).

The REA method is based on sampling upward and downward moving eddies at constant flow rates, which relies on an ultrasonic anemometer to detect the vertical wind velocity and control the fast response valves. The GEM dry deposition flux based on the REA method is calculated as follows:

$$F_{\mathrm{dry,REA}} = \beta\sigma_w(C_{\mathrm{down}} - C_{\mathrm{up}}) \quad (4)$$

where $F_{\mathrm{dry,REA}}$ is the GEM dry deposition flux measured by the REA method, β is relaxation coefficient, σ_w is the standard deviation of the vertical wind speed, and

Atmos. Chem. Phys. Discuss., https://doi.org/10.5194/acp-2019-347
Manuscript under review for journal Atmos. Chem. Phys.
Discussion started: 13 May 2019
© Author(s) 2019. CC BY 4.0 License.

Atmospheric Chemistry and Physics Discussions

C_{down} and C_{up} are the downward and upward GEM concentration, respectively.

The REA method conducts upward and downward sampling at the same height, eliminating the footprint difference and potential GEM formation and loss (Zhu et al., 2016). Dual inlets were recommended and applied in recent studies due to advantages of synchronous concentration determination (Sommar et al., 2013b; Zhu et al., 2015b; Kamp et al., 2018; Osterwalder et al., 2018).

The gradient methods (AER and MBR) sample air at different height to get the vertical GEM concentration gradient. For the AER method, the GEM dry deposition flux is calculated using the following equation (Fritsche et al., 2008; Baya and Van Heyst, 2010; Yu et al., 2018):

$$F_{dry,AER} = K\frac{\partial C}{\partial z} \quad (5)$$

where $F_{dry,AER}$ is the GEM dry deposition flux measured by the AER method, K is the turbulent transfer coefficient (Yu et al., 2018), and $\partial C/\partial z$ is the gradient of the vertical GEM concentration.

For the MBR method, the GEM dry deposition flux is calculated based on the theory that the ratio of GEM and the reference scalar (e.g., H_2O) fluxes is proportional to their concentration gradients (Obrist et al., 2006; Converse et al., 2010; Zhu et al., 2015a):

$$F_{dry,MBR} = F_r\frac{\partial C_{Hg}}{\partial C_r} \quad (6)$$

where $F_{dry,MBR}$ is the GEM dry deposition flux measured by the MBR method, F_r is the flux of the reference scalar, and $\partial C_{Hg}/\partial C_r$ is the concentration gradient ratio of GEM over the reference scalar.

Micrometeorological methods are relatively reliable with high temporal resolution and represent the ecosystem scale due to less interference from the microenvironment (Zhu et al., 2016). The direct flux measurement methods generally have more complex installment and high expenses than the gradient methods, but could reduce uncertainties due to the elimination of the sampling height difference (Sommar et al., 2013b; Pierce et al., 2015).

2.2 Methods for Hg wet deposition

Hg wet deposition through precipitation is easier to measure than dry deposition and usually more reliable. The Hg wet deposition flux is calculated as follows:

Atmos. Chem. Phys. Discuss., https://doi.org/10.5194/acp-2019-347
Manuscript under review for journal Atmos. Chem. Phys.
Discussion started: 13 May 2019
© Author(s) 2019. CC BY 4.0 License.

Atmospheric Chemistry and Physics Discussions

$$F_{\text{wet}} = \sum_{i=1}^{n} C_i \cdot D_i \quad (7)$$

where F_{wet} is the total Hg wet deposition flux, n is the number of precipitation events during a certain period, C_i is the total Hg concentration in precipitation water during Event i, and D_i is the precipitation depth of Event i.

Both manual and automatic precipitation sample collectors were used in previous studies (Fu et al., 2010a; Gratz and Keeler, 2011; Marumoto and Matsuyama, 2014; Zhu et al., 2014; Brunke et al., 2016; Chen et al., 2018). Automatic precipitation sample collectors cover the lid automatically when it is not raining to prevent potential contamination, while manual collectors require manually placing collectors before precipitation events and retrieving them after events. All collector sections exposed to rainwater should be made by teflon or borosilicate glass due to potential Hg adsorption (Fu et al., 2016). The collected samples need to be acidified and then preserved in a cool and dark environment before analysis. The total Hg concentration in precipitation water is analyzed by oxidation, purge and trap, and cold vapor atomic fluorescence spectrometry (CVAFS) following EPA Method 1631E. GOM and PBM are the main Hg forms removed by precipitation due to high solubility. Usually, GOM and PBM contribute equivalently to Hg wet deposition (Cheng et al., 2015).

2.3 Methods for Hg deposition in forests

In forest ecosystems, Hg dry and wet depositions are not able to be distinguished markedly. Litterfall and throughfall are commonly used to evaluate the Hg deposition in forests (Wang et al., 2016b; Wright et al., 2016). Cloud and fog are also important forms of Hg deposition in forest regions, especially at high-elevation sites (Blackwell and Driscoll, 2015).

2.3.1 Litterfall

Hg dry deposition in forests includes uptake of Hg by leaf stomata and cuticle, tree bark, and underlying soil. Some of the deposited Hg in the soil may emit back into the atmosphere and be captured by leaves, while some of the deposited Hg in leaves may be translocated to branches, stems and roots. Litterfall Hg deposition includes the remaining dry-deposited Hg in leaves and bark as well as the captured Hg emitted from the soil (Blackwell and Driscoll, 2015; Wright et al., 2016). Litterfall Hg deposition flux is calculated as follows:

Atmos. Chem. Phys. Discuss., https://doi.org/10.5194/acp-2019-347
Manuscript under review for journal Atmos. Chem. Phys.
Discussion started: 13 May 2019
© Author(s) 2019. CC BY 4.0 License.

Atmospheric Chemistry and Physics Discussions

$$F_{\text{litterfall}} = \frac{E_A \cdot C_l \cdot M_l}{A \cdot t} \quad (8)$$

where $F_{\text{litterfall}}$ is the litterfall Hg deposition flux, E_A is the litterfall trap area expansion factor, C_l is the Hg mass concentration in litterfall, M_l is the total dry weight of litterfall, A is the litterfall trap area, and t is the sampling time (Fisher and Wolfe, 2012).

Litterfall is collected during the leaf-growing or -falling seasons with litterfall traps or collectors (Fisher and Wolfe, 2012). It should be noted that the Hg concentration in leaves has an approximately linear correlation with time during the growing season (Bushey et al., 2008; Fu et al., 2010a; Gong et al., 2014). Litterfall is collected on a regular basis to prevent potential weight loss and changes in chemical composition caused by rain leaching and decomposition. The litterfall samples collected are then air-dried, ground and stored under a low temperature and dark environment for analysis (Zhou et al., 2017). The Hg content in litterfall can be determined by thermal decomposition, amalgamation, and cold vapor atomic absorption spectrophotometry (CVAAS) following EPA Method 7473 (Richardson and Friedland, 2015; Fu et al., 2016; Zhou et al., 2017; Risch et al., 2017). Alternatively, the litterfall samples can be digested into solution, and the extracted Hg in the solution can be analyzed following EPA Method 1631E (Fu et al., 2010a; Fisher and Wolfe, 2012).

2.3.2 Throughfall

Throughfall Hg deposition includes wet-deposited Hg above the canopy and a portion of dry-deposited Hg washed off from the canopy (Blackwell and Driscoll, 2015; Wright et al., 2016). Throughfall Hg deposition flux is calculated as follows:

$$F_{\text{throughfall}} = \frac{E_A \cdot C_t \cdot V_t}{A \cdot t} \quad (9)$$

where $F_{\text{throughfall}}$ is the throughfall Hg deposition flux, E_A is the throughfall funnel area expansion factor, C_t is the Hg mass concentration in throughfall, V_t is the total volume of throughfall, A is the throughfall funnel area, and t is the sampling time (Fisher and Wolfe, 2012).

Throughfall under canopy is usually collected using a passive bulk throughfall collector with a funnel connected a bottle for water storage (Wang et al., 2009; Fisher and Wolfe, 2012; Åkerblom et al., 2015) or collected as open-field rain collection if the environmental condition permits (Choi et al., 2008; Fu et al., 2010a; Fu et al., 2010b; Han et al., 2016). Attention should be paid to potential litterfall contamination

© Author(s) 2019. CC BY 4.0 License.

and cloud/fog deposition influence at high elevation sites if the collector is not sheathed (Fisher and Wolfe, 2012; Wright et al., 2016). Throughfall samples are usually analyzed following EPA Method 1631E (Fisher and Wolfe, 2012).

2.3.3 Cloud/fog

At high elevation sites, besides litterfall and throughfall deposition, cloud/fog Hg deposition could account for a large proportion of the total deposition (Lawson et al., 2003; Sheu and Lin, 2011; Stankwitz et al., 2012; Blackwell and Driscoll, 2015). Quantifying Hg in cloud/fog at high elevation helps better understand the impact of long-range transport and local sources on global Hg cycling (Malcolm et al., 2003). Both active and passive collectors are used to collect cloud/fog. The passive collector has two round disks with teflon wires strung in between. Cloud/fog water collides onto the teflon wires and slides down to a sampling bottle (Lawson et al., 2003; Malcolm et al., 2003; Sheu and Lin, 2011; Schwab et al., 2016). Active cloud/fog water samplers use a fan to blow cloud/fog to teflon strings which are used to gather cloud/fog droplets (Kim et al., 2006; Weiss-Penzias et al., 2018). The collected cloud/fog water samples are usually analyzed using EPA Method 1631E (Blackwell and Driscoll, 2015). Cloud/fog Hg deposition flux is calculated as follows:

$$F_{\text{cloud/fog}} = F_d \cdot C_{\text{Hg}} \quad (10)$$

where $F_{\text{cloud/fog}}$ is the cloud/fog Hg deposition flux, F_d is the deposition flux of cloud/fog, and C_{Hg} is the Hg concentration in cloud/fog. F_d can be estimated using resistance models, analytical models or sophisticated atmosphere-soil-vegetation models (Katata, 2014).

3 Models for Hg dry deposition

Dry deposition fluxes of speciated Hg can also be estimated by coupling speciated Hg concentrations and dry deposition models (Wright et al., 2016). Here we summarize dry deposition models for different Hg forms.

3.1 Resistance model for GOM

It is assumed that GOM dry deposition flux is proportional to the GOM concentration (Seinfeld and Pandis, 2016):

$$F_{\text{dry,GOM}} = v_d \cdot C_z \quad (11)$$

where $F_{\text{dry,GOM}}$ is the GOM dry deposition flux, C_z is the GOM concentration at reference height z, and v_d is the dry deposition velocity which can be calculated using

Atmos. Chem. Phys. Discuss., https://doi.org/10.5194/acp-2019-347
Manuscript under review for journal Atmos. Chem. Phys.
Discussion started: 13 May 2019
© Author(s) 2019. CC BY 4.0 License.

the following equation:

$$v_d = \frac{1}{R_a + R_b + R_c} \quad (12)$$

where R_a is the aerodynamic resistance depending on the meteorological conditions and the land use category, R_b is the quasi-laminar resistance, a function of friction velocity and the molecular diffusivity of each chemical species (Zhang et al., 2002), and R_c is the canopy resistance which can be further parameterized as follows:

$$R_c = \left(\frac{1 - W_{st}}{R_{st} + R_m} + \frac{1}{R_{ns}} \right)^{-1} \quad (13)$$

where W_{st} is the fraction of stomatal blocking under wet conditions, R_{st} is the stomatal resistance, R_m is the mesophyll resistance, and R_{ns} is the non-stomatal resistance which is comprised of in-canopy, soil, and cuticle resistances. Cuticle and soil resistances for GOM can be scaled to those of SO_2 and O_3 using the following equation:

$$R_{x,\mathrm{GOM}} = \left(\frac{\alpha_{\mathrm{GOM}}}{R_{x,\mathrm{SO_2}}} + \frac{\beta_{\mathrm{GOM}}}{R_{x,\mathrm{O_3}}} \right)^{-1} \quad (14)$$

where R_x is the cuticle or soil resistance, α and β are two scaling parameters (Zhang et al., 2003; Zhang et al., 2012). Among the numerous parameters in the resistance model the two scaling factors for the non-stomatal resistance components regarding the solubility and reactivity of the chemical species are the most sensitive ones. The values for HNO_3 (α=β=10) used to be applied in the model for GOM (Marsik et al., 2007; Castro et al., 2012; Zhang et al., 2012). However, some other studies found the values for HONO (α=β=2) are probably more suitable for GOM due to equivalent effective Henry's Law constants (H^*) between HONO and $HgCl_2$ (Lyman et al., 2007). Huang and Gustin (2015) indicated that no single value could be used to calculate GOM dry deposition due to the unknown GOM compounds. Various values for the two scaling parameters (α=β=2, 5, 7 and 10) were used in Huang et al. (2017) to identify dominant GOM deposition species.

3.2 Resistance model for PBM

For PBM dry deposition, a size-segregated resistance model is more and more widely applied, based on the theory that v_d for atmospheric particles strongly depend on particle size distributions (Dastoor and Larocque, 2004; Zhang et al., 2009; Zhang and He, 2014). Many independent studies (Fang et al., 2012; Zhu et al., 2014) showed that

Atmos. Chem. Phys. Discuss., https://doi.org/10.5194/acp-2019-347
Manuscript under review for journal Atmos. Chem. Phys.
Discussion started: 13 May 2019
© Author(s) 2019. CC BY 4.0 License.

Atmospheric Chemistry and Physics Discussions

316 Hg in coarse particles constitutes a large mass fraction of the total PBM, which was
317 previously neglected. PBM measured by Tekran 2537/1130/1135 only considers fine
318 particles. Based on available measurements of PBM size distributions and fine/coarse
319 PBM mass ratios, Zhang et al. (2016b) assumed 30% of the total PBM mass to be
320 coarse particles in order to estimate total PBM dry deposition flux based on the theory
321 that PBM has the same proportion in both fine and course particles.

322 The total PBM dry deposition can be calculated as follows:

323 $$F_{\mathrm{dry,PBM}} = C_f \left(v_f + \frac{f}{1-f} v_c \right) \quad (15)$$

324 where $F_{\mathrm{dry,PBM}}$ is the total PBM dry deposition flux, C_f is the mass concentration of
325 PBM in fine particles, v_f and v_c are the dry deposition velocities of PBM for fine and
326 coarse particles, respectively, and f is the mass fraction of PBM in coarse particles. v_f
327 and v_c can be calculated using the following equation:

328 $$v_x = v_g + \frac{1}{R_a + R_s} \quad (16)$$

329 where v_x is v_f or v_c, v_g is the gravitational settling velocity, R_a is the aerodynamic
330 resistance, and R_s is the surface resistance which can be parameterized as a function of
331 collection efficiencies from Brownian diffusion, impaction, and interception
332 mechanisms (Zhang et al., 2012; Zhang et al., 2016b). Zhang and He (2014) have
333 developed an easier bulk algorithm based on the v_x scheme of Zhang et al. (2001) to
334 make this model more widely applicable in monitoring networks.

335 **3.3 Bidirectional air-surface exchange model for GEM**

336 GEM dry deposition can also be calculated using the resistance model with different
337 parameters. However, the re-emission and natural emission of GEM must be taken
338 into consideration. Net GEM dry deposition is estimated from the difference between
339 the estimated unidirectional deposition flux and the modeled total re-emission plus
340 natural emission in the resistance model (Zhang et al., 2012).

341 A bidirectional air-surface exchange model modified from the resistance model is
342 more and more recommended in recent years (Zhang et al., 2009; Bash, 2010; Wang
343 et al., 2014; Zhang et al., 2016b; Zhu et al., 2016). In the bidirectional scheme, the
344 GEM dry deposition flux can be calculated as follows:

345 $$F_{\mathrm{dry,GEM}} = \frac{\chi_a - \chi_c}{R_a + R_b} \quad (17)$$

Atmos. Chem. Phys. Discuss., https://doi.org/10.5194/acp-2019-347
Manuscript under review for journal Atmos. Chem. Phys.
Discussion started: 13 May 2019
© Author(s) 2019. CC BY 4.0 License.

Atmospheric Chemistry and Physics Discussions

$$\chi_c = \left(\frac{\chi_a}{R_a + R_b} + \frac{\chi_{st}}{R_{st} + R_m} + \frac{\chi_g}{R_{ac} + R_g} \right) \left(\frac{1}{R_a + R_b} + \frac{1}{R_{st} + R_m} + \frac{1}{R_{ac} + R_g} + \frac{1}{R_{cut}} \right)^{-1} \quad (18)$$

where $F_{\mathrm{dry,GEM}}$ is the net GEM dry deposition flux; χ_a is the GEM concentration at a reference height; R_a, R_b, R_{st}, R_m, R_{ac}, R_g and R_{cut} are aerodynamic, quasi-laminar, stomatal, mesophyll, in-canopy aerodynamic, ground surface and cuticle resistances, respectively (Zhang et al., 2016b); and χ_{st} and χ_g are canopy, stomatal and ground surface compensation points, respectively. Based on observations on different land use categories, Wright and Zhang (2015) have proposed a range of χ_{st} and χ_g.

4 Global observation network of Hg deposition

There have been several observation networks of Hg wet deposition. The Global Mercury Observation System (GMOS) is so far the only global scale network covering the northern hemisphere, the tropics, and the southern hemisphere (Sprovieri et al., 2017). The Mercury Deposition Network (MDN) of the National Atmospheric Deposition Program (NADP) in North America is the earliest continental scale network specifically for Hg deposition (Prestbo and Gay, 2009; Weiss-Penzias et al., 2016). Hg wet deposition is also monitored in the European Monitoring and Evaluation Programme (EMEP) for Europe (Tørseth et al., 2012; Bieser et al., 2014). A new Asia–Pacific Mercury Monitoring Network has recently been established (Obrist et al., 2018). Since the methods of measurements still have high uncertainties, there is not yet any tangible monitoring network for Hg dry deposition.

4.1 Wet deposition

Sprovieri et al. (2017) reported a 5-year record (2011–2015) of Hg wet deposition at 17 selected GMOS monitoring sites, which provided a global baseline of the Hg wet deposition flux including regions in the southern hemisphere and tropical areas where Hg wet deposition had never been investigated before. The average Hg wet deposition fluxes in the northern hemisphere, the tropics, and the southern hemisphere were 2.9 (0.2–6.7), 4.7 (2.4–7.0), and 1.9 (0.3–3.3) μg m^{-2} yr^{-1}, respectively. Precipitation volume was found to be the key factor for the inter-annual differences in total Hg wet deposition. The MDN network has a much longer history which dates back to the 1990s. Weiss-Penzias et al. (2016) analyzed records from 19 sites in the United States (U.S.) and Canada between 1997 and 2013, and discovered trends of Hg concentration in wet deposition, with the early time period (1998–2007) producing a significantly

© Author(s) 2019. CC BY 4.0 License.

negative trend (−1.5±0.2% yr^{-1}) and the late time period (2008–2013) a flat slope (not significant). Therefore, the MDN data of 136 sites (http://nadp.slh.wisc.edu/mdn) for the time period of 2008–2015 was summarized in this study to represent the recent background Hg wet deposition level in North America. Fu et al. (2016) summarized wet deposition measurements from 7 monitoring sites in China. Hg wet deposition fluxes at rural sites in forest and grassland were averagely 6.2 and 2.0 μg m^{-2} yr^{-1}, respectively, while the flux at an urban site was as high as 12.6±6.5 μg m^{-2} yr^{-1}.

Figure 1 summarizes the global distribution of Hg wet deposition based on existing studies. Hg wet deposition flux is not significantly related to elevation. Overall, East Asia has the highest wet deposition flux (averagely 16.1 μg m^{-2} yr^{-1}), especially in the southern part of China where the GEM concentration level is relatively high (Fu et al., 2008; Guo et al., 2008; Wang et al., 2009; Fu et al., 2010; Ahn et al., 2011; Huang et al., 2012; Seo et al., 2012; Huang et al., 2013; Sheu and Lin, 2013; Marumoto and Matsuyama, 2014; Xu et al., 2014; Zhu et al., 2014; Huang et al., 2015; Zhao et al., 2015; Han et al., 2016; Fu et al., 2016; Ma et al., 2016; Nguyen et al., 2016; Qin et al., 2016; Sommar et at., 2016; Cheng et al., 2017; Chen et al., 2018; Lu and Liu, 2018). North America has the most complete deposition observation network with an average Hg wet deposition flux of 9.1 μg m^{-2} yr^{-1}, and exhibits a decreasing spatial profile from the southeastern part to the northwestern part, which is consistent with the distribution of the atmospheric Hg concentration (Zhang et al., 2012; Gichuki and Mason, 2014; Lynam et al., 2017). Europe has the lowest Hg wet deposition flux (averagely 3.4 μg m^{-2} yr^{-1}) according to the available dataset (Connan et al., 2013; Bieser et al., 2014; Siudek et al., 2016). Observation sites in the tropics and the southern hemisphere are scarce with large variation in Hg wet deposition flux (Wetang'ula, 2011; Gichuki and Manson, 2013; Sprovieri et al., 2017). Precipitation could be the main cause of the differences.

The relationship between the annual precipitation and the Hg wet deposition flux is shown in Fig. 2. The wet deposition flux is basically positively related to the annual precipitation, except for 8 sites in southwestern China which are close to former Hg mining area and 3 urban or suburban sites in southeastern China. These 11 sites have an average Hg wet deposition flux of 34.5 μg m^{-2} yr^{-1}. The one exceptional tropical site with a wet deposition flux of 16.8 μg m^{-2} yr^{-1} is in Kenya while the other sites in the tropics are all in Mexico (Wetang'ula, 2011; Hansen and Gay, 2013). The two sites

© Author(s) 2019. CC BY 4.0 License.

in the southern hemisphere with annual precipitation of over 4000 mm are in Australia and have wet deposition fluxes of 29.1 and 18.2 μg m^{-2} yr^{-1}, respectively (Dutt et al., 2009). The slope of the relationship implies the Hg concentration in precipitation. Europe has the flattest slope among all regions, indicating its lowest Hg pollution level around the world.

4.2 Dry deposition

The Hg dry deposition network is immature compared to the wet deposition network due to the inconsistency in methods of measurements. GOM dry deposition fluxes were either measured by the surrogate surface method using CEMs or estimated from measurements of GOM concentrations. PBM dry deposition fluxes were mainly estimated from the measurements of total or size-resolved PBM concentrations. GEM dry deposition fluxes were measured by different types of methods, the surrogate surface methods, the enclosure methods, and the micrometeorological methods.

Figure 3 shows the global distribution of the GOM, PBM and GEM dry deposition fluxes. Although large uncertainties still exist in the methods for Hg dry deposition measurements, it should be noted that GEM dry deposition is non-negligible compared to GOM and PBM.

The data of GOM dry deposition fluxes concentrate in North America and Europe, among which direct observations of GOM dry deposition are mainly from North America (Lyman et al., 2007; Lyman et al., 2009; Weiss-Penzias et al., 2011; Lombard et al., 2011; Castro et al., 2012; Gustin et al., 2012; Peterson et al., 2012; Zhang et al., 2012; Sather et al., 2013; Bieser et al., 2014; Huang et al., 2014; Sather et al., 2014; Wright et al., 2014; Huang and Guatin, 2015; Enrico et al., 2016; Han et al., 2016; Zhang et al., 2016; Huang et al., 2017). Regardless of the evaluating methods, the mean GOM dry deposition flux in North America (6.4 μg m^{-2} yr^{-1}) is higher than in Europe (3.0 μg m^{-2} yr^{-1}). Han et al. (2016) used knife-edge surrogate surface (KSS) samplers with quartz filters to measure GOM dry deposition at a remote site in Korea, and found an average GOM dry deposition flux of 4.78 μg m^{-2} yr^{-1}. Huang et al. (2012a) used KSS samplers with CEMs in several polluted areas and got a much higher average (52.9 μg m^{-2} yr^{-1}). A significant correlation (R^2=0.532, $p<0.01$) was found between the elevation and the GOM dry deposition flux (Fig. 4). Huang and Gustin (2014) found that measured dry deposition of GOM was significantly high at sites over 2000 m above sea level, and attributed it to high GOM concentrations at

© Author(s) 2019. CC BY 4.0 License.

high elevation and atmospheric turbulence.

Due to the severe particulate matter (PM) pollution in East Asia, many independent size-resolved PM measurements were conducted in recent years with analysis of Hg in PM accordingly. Results from size-resolved PBM analysis and PBM dry deposition models show that East Asia has a much higher average of PBM dry deposition flux (45.3 μg m^{-2} yr^{-1}) than North America (1.1 μg m^{-2} yr^{-1}) with coarse-particle PBM dry deposition not considered (Fang et al., 2012a; Fang et al., 2012b; Zhu et al., 2014; Zhang et al., 2015; Huang et al., 2016; Guo et al., 2017).

The mean GEM dry deposition is lower in Europe (4.3±8.1 μg m^{-2} yr^{-1}) while higher and more variable in North America (5.2±15.5 μg m^{-2} yr^{-1}) (Castelle et al., 2009; Baya and Heyst, 2010; Converse et al., 2010; Miller et al., 2011). The four Asian sites using micrometeorological methods all show negative values (−36.3±19.6 μg m^{-2} yr^{-1}) (Luo et al., 2015; Luo et al., 2016; Ci et al., 2016; Sommar et al., 2016), indicating natural GEM emission sources rather than GEM deposition sinks, but the GEM dry deposition data in Asia is very limited. No GEM, GOM or PBM dry deposition data were found for the tropics or the southern hemisphere.

Large uncertainties still exist in the evaluating methods. Significant discrepancies were found between observed and simulated GOM dry deposition fluxes (Fig. 5). Some recent studies used a scaling factor of 3 to adjust GOM concentrations (Huang and Gustin, 2014; Huang et al., 2017), trying to offset the underestimation due to the low capture efficiency of the widely adopted KCl denuder method for measurements of GOM concentrations (Huang and Gustin, 2015).

4.3 Forest deposition

Hg deposition in forests is mainly in the form of litterfall and throughfall. Wang et al. (2016) made a comprehensive assessment of the global Hg deposition through litterfall, and found litterfall Hg deposition an important input to terrestrial forest ecosystems (1180±710 Mg yr^{-1}). South America was estimated to bear the highest litterfall Hg deposition (65.8±57.5 μg m^{-2} yr^{-1}) around the world. This was partially because some studies were conducted in the Amazonian rainforest (Fostier et al., 2015), mainly semi-deciduous or evergreen tropical forest, which account for over 40% litterfall deposition globally (Shen et al., 2019). Another reason was that some sampling sites were very close to large cities or polluted areas, which could lead to more Hg accumulation (Teixeira et al., 2012; Buch et al., 2015; Teixeira et al., 2017;

© Author(s) 2019. CC BY 4.0 License.

476 Fragoso et al., 2018). There have been numerous forest Hg deposition studies in the
477 recent decade in East Asia with the second highest average litterfall Hg deposition
478 flux (35.5±27.7 μg m^{-2} yr^{-1}). The forest type varies among different studies, but East
479 Asia has much higher Hg concentrations in litterfall (42.9–62.8 ng/g) compared to
480 other regions (Wan et al., 2009; Wang et al., 2009; Fu et al., 2010a; Fu et al., 2010b;
481 Gong et al., 2014; Luo et al., 2015; Ma et al., 2015; Han et al., 2016; Fu et al., 2016;
482 Ma et al., 2016; Wang et al., 2016; Zhou et al., 2016; Zhou et al., 2017). Lower levels
483 of litterfall Hg deposition fluxes were found in North America (12.3±4.9 μg m^{-2} yr^{-1})
484 and Europe (14.4±5.8 μg m^{-2} yr^{-1}) (Larssen et al., 2008; Obrist et al., 2009; Fisher and
485 Wolfe, 2012; Juillerat et al., 2012; Obrist et al., 2012; Benoit et al., 2013; Navrátil et
486 al., 2014; Gerson et al., 2017; Risch et al., 2017; Risch and Kenski, 2018). According
487 to Risch et al. (2017), the litterfall Hg deposition flux in the eastern U.S. decreased
488 year by year during 2007–2014 with a decline rate of 0.8 μg m^{-2} yr^{-1}. From 2007 to
489 2009 the decrease occurred more rapidly due to the Hg emission control strategies
490 during this period of time.

491 Most studies on Hg deposition in forests in North America use rainfall instead of
492 throughfall since dry deposition in North American forests has limited contribution
493 (Risch et al., 2017), while Asian studies found large discrepancy between throughfall
494 and rainfall Hg deposition fluxes (32.9±18.9 and 13.3±8.6 μg m^{-2} yr^{-1}, respectively),
495 indicating a high dry deposition level in Asian forests (Wan et al., 2009; Wang et al.,
496 2009; Fu et al., 2010a; Fu et al., 2010b; Luo et al., 2015; Ma et al., 2015; Han et al.,
497 2016; Fu et al., 2016; Ma et al., 2016; Wang et al., 2016; Zhou et al., 2016). Litterfall
498 and throughfall Hg deposition fluxes are equivalent. Wright et al. (2016) summarized
499 previous studies and reported the mean litterfall and throughfall Hg deposition,
500 respectively, 42.8 and 43.5 μg m^{-2} yr^{-1} in Asia, 14.2 and 19.0 μg m^{-2} yr^{-1} in Europe,
501 and 12.9 and 9.3 μg m^{-2} yr^{-1} in North America.

502 Studies of cloud/fog Hg deposition are very limited so far. Stankwitz et al. (2012)
503 and Gerson et al. (2017) found the average cloud/fog Hg deposition fluxes of two
504 North American forests to be 7.4 and 4.3 μg m^{-2} yr^{-1}, respectively. In California
505 coastline, fog Hg deposition, with only 2% volume proportion, accounts for 13% of
506 the total wet deposition (Weiss-Penzias et al., 2016). At high-elevation observatories
507 the contribution of cloud/fog Hg deposition is non-negligible. Converse et al. (2014)
508 found the annual Hg deposition to dew/frost at a high-elevation site in the U.S. to be

© Author(s) 2019. CC BY 4.0 License.

about 0.12 μg m^{-2} yr^{-1}, 2–3 orders of magnitude smaller than wet deposition. More studies and a more standardized method for cloud/fog water sampling are needed.

5 Global Hg deposition on different terrestrial surfaces

Terrestrial surface type is a key factor for global Hg deposition. We summarized existing studies to make comparisons for Hg deposition on different terrestrial surfaces. Figures 6–8 exhibit wet, dry, and litterfall Hg deposition fluxes for different terrestrial surface types.

As shown in Fig. 6a, the average Hg wet deposition flux follows the ascending sequence of grasslands, croplands, savannas, and urban areas, which is mainly linked to the precipitation levels on these surfaces. Barren areas have the lowest Hg wet deposition flux due to their lowest precipitation. Water surfaces, e.g., coastal, offshore, and lakeside sites, have a lower wet deposition level than the surfaces with a similar amount of precipitation. This is possibly related to fog deposition. The relatively low Hg concentration in precipitation on water surfaces could be caused by fog scavenging, not only in high-elevation regions, but also in the near water areas. Fog deposition is not considered in Hg wet deposition. Forests have a similar precipitation level as urban areas, but exhibit much lower wet deposition fluxes. This is probably because most forests are in remote areas with low total atmospheric Hg concentration levels. It is the reactive Hg (GOM and PBM) that determines the Hg concentration in precipitation. Hg wet deposition fluxes for different forest types are shown in Fig. 6b. Forests have a similar precipitation level. The high wet deposition fluxes for deciduous needle leaf and evergreen broadleaf forests are both induced by samples from Chongqing, a city with a relatively high atmospheric Hg concentration in China (Wang et al., 2009; Qin et al., 2016). In general, the Hg wet deposition flux does not vary significantly among the five forest types.

The distribution of Hg dry deposition on various terrestrial surfaces is quite different among the three atmospheric Hg forms (Fig. 7). GEM dry deposition is equivalent to GOM and PBM dry deposition, even significantly higher than in forests. As shown in Fig. 7a, the Hg oxidation process plays a more important role at sites with higher elevations (more halogen free radicals) or more intensive solar radiations, resulting in high GOM dry deposition levels for grasslands (including alpine meadow) and savannas, respectively. Urban areas with high GOM concentrations also have relatively high GOM dry deposition fluxes. The low GOM dry deposition fluxes on

© Author(s) 2019. CC BY 4.0 License.

moist surfaces (water and croplands) might be partially because of dew/fog scavenging (Malcolm and Keeler. 2002; Zhang et al., 2009). The PBM dry deposition flux is high on surfaces with high human activities (urban areas and croplands) and low in vegetative areas implying the heavier PM pollution in urban and rural areas than in remote areas (Fig. 7b). Agnan et al. (2015) and Zhu et al. (2016) made detailed summaries of campaign-based GEM dry deposition observations, and addressed the importance of natural Hg emission sources. Due to the lack of long-term observations (no less than one year), we summarized model evaluations and one annual observation dataset (Zhang et al., 2012; Bieser et al., 2014; Zhang et al., 2016; Enrico et al., 2016), and found that the GEM dry deposition does not only depend on GEM concentration, but also on the air–soil Hg exchange compensation point. Regarding the annual air–surface Hg exchange, instead of an important natural source, forests tend to be a net sink of atmospheric Hg (Fig. 7c). Therefore, long-term studies of GEM dry deposition are of urgent need.

The litterfall Hg deposition flux and the Hg concentration in litterfall are shown in Fig. 8. In general, evergreen forests have higher litterfall Hg concentrations than deciduous forests due to longer accumulation time (Wright et al., 2016). Evergreen broadleaf forests have not only high litterfall Hg concentrations but also high litterfall rates (Shen et al., 2019), and consequently exhibit significantly high litterfall Hg deposition fluxes. Comparing the levels of wet, dry, and litterfall Hg depositions in forests, litterfall markedly takes the lead, especially for evergreen broadleaf forests. This is consistent with the budget of global litterfall Hg deposition developed by Wang et al. (2016a).

6 Summary and recommendations

Hg wet and dry depositions to terrestrial surfaces, as well as litterfall, throughfall and cloud/fog depositions in forests, have been measured globally over the last two decades to improve our understanding on the sink of atmospheric Hg. Owing to the unified and reliable methodology, a global Hg wet deposition monitoring network has been established, especially the matured network in North America. Dry deposition of speciated atmospheric Hg (GEM, GOM and PBM), however, has diverse methods for measurements, including the surrogate surface methods, the enclosure methods, and the micrometeorological methods. For the Hg deposition forms in forests, litterfall and throughfall are easy to observe, while the measurements of cloud/fog deposition are

© Author(s) 2019. CC BY 4.0 License.

still preliminary. The Hg dry deposition flux can also be estimated based on speciated Hg concentrations in the atmosphere using resistance models or bidirectional air–surface exchange models. Key parameters (e.g., the two scaling factor, α and β, for cuticle or soil resistance) still generate large uncertainties. The land use category is an important factor in modeling Hg deposition. Therefore, we compared the data for different terrestrial surfaces. Water surfaces could affect Hg wet deposition through fog scavenging. Hg wet deposition is an indicator of the atmospheric Hg pollution level for a certain region. Altitude is a key factor for GOM dry deposition. GEM dry deposition is non-negligible compared to GOM and PBM dry deposition, especially for forests. Litterfall could be the dominant form of Hg deposition in forests.

Based on current understanding on global Hg deposition, we think future research needs lie in the following aspects:

(1) Different chemical forms of GOM (e.g., $HgCl_2$, $HgBr_2$, $HgSO_4$, etc.) could have different dry deposition velocities. Quantification methods for concentrations of different GOM species need to be developed to improve the evaluation of the Hg dry deposition flux, which has much higher uncertainty than the wet, litterfall, and throughfall deposition fluxes.

(2) The resistance model for GOM dry deposition requires better parameterization considering different GOM species. Moreover, the model should utilize more accurate GOM concentration data. The KCl denuder-based method for GOM measurements has significant underestimation caused by high humidity or ozone concentration.

(3) The contribution GEM dry deposition has been underestimated previously. Inter-comparison between different methods for GEM dry deposition measurements needs to be conducted to determine a unified method for monitoring networks.

(4) Cloud, fog or even dew Hg deposition needs careful investigation which requires more standardized sampling methods. At high-elevation sites cloud/fog Hg deposition should be included in the total wet deposition.

Author contribution. Dr. Lei Zhang designed the review framework. Dr. Lei Zhang and Peisheng Zhou did the most literature review work with contributions from Shuzhen Cao and Dr. Yu Zhao. Dr. Lei Zhang prepared the manuscript with contributions from all co-authors.

© Author(s) 2019. CC BY 4.0 License.

Acknowledgements. This review work was supported by the National Natural Science Foundation of China (No. 21876077) and the Fundamental Research Funds for the Central Universities (No. 14380080 and No. 14380092).

References

Agnan, Y., Le Dantec, T., Moore, C. W., Edwards, G. C., and Obrist, D.: New constraints on terrestrial surface atmosphere fluxes of gaseous elemental mercury using a global database, Environ. Sci. Technol., 50, 507–524, 10.1021/acs.est5b04013, 2016.

Ahn, M. C., Yi, S. M., Holsen, T. M., and Han, Y. J.: Mercury wet deposition in rural Korea: concentrations and fluxes, J. Environ. Monit., 13, 2748–2754, 10.1039/c1em10014a, 2011.

Åkerblom, S., Meili, M., and Bishop, K.: Organic matter in rain: an overlooked influence on mercury deposition, Environ. Sci. Technol. Lett., 2, 128–132, 10.1021/acs.estlett.5b00009, 2015.

Bash, J. O.: Description and initial simulation of a dynamic bidirectional air-surface exchange model for mercury in Community Multiscale Air Quality (CMAQ) model, J. Geophys. Res., 115, 10.1029/2009jd012834, 2010.

Baya, A. P., and Van Heyst, B.: Assessing the trends and effects of environmental parameters on the behaviour of mercury in the lower atmosphere over cropped land over four seasons, Atmos. Chem. Phys., 10, 8617–8628, 10.5194/acp-10-8617-2010, 2010.

Benoit, J. M., Cato, D. A., Denison, K. C., and Moreira, A. E.: Seasonal mercury dynamics in a New England vernal pool, Wetlands, 33, 887–894, 10.1007/s13157-013-0447-4, 2013.

Bieser, J., De Simone, F., Gencarelli, C., Geyer, B., Hedgecock, I., Matthias, V., Travnikov, O., and Weigelt, A.: A diagnostic evaluation of modeled mercury wet depositions in Europe using atmospheric speciated high-resolution observations, Environ. Sci. Pollut. Res., 21, 9995–10012, 10.1007/s11356-014-2863-2, 2014.

Blackwell, B. D., and Driscoll, C. T.: Using foliar and forest floor mercury concentrations to assess spatial patterns of mercury deposition, Environ. Pollut., 202, 126–134, 10.1016/j.envpol.2015.02.036, 2015a.

Blackwell, B. D., and Driscoll, C. T.: Deposition of mercury in forests along a

© Author(s) 2019. CC BY 4.0 License.

montane elevation gradient, Environ. Sci. Technol., 49, 5363–5370, 10.1021/es505928w, 2015b.

Brunke, E.-G., Walters, C., Mkololo, T., Martin, L., Labuschagne, C., Silwana, B., Slemr, F., Weigelt, A., Ebinghaus, R., and Somerset, V.: Mercury in the atmosphere and in rainwater at Cape Point, South Africa, Atmos. Environ., 125, 24–32, 10.1016/j.atmosenv.2015.10.059, 2016.

Buch, A. C., Correia, M. E., Teixeira, D. C., and Silva-Filho, E. V.: Characterization of soil fauna under the influence of mercury atmospheric deposition in Atlantic Forest, Rio de Janeiro, Brazil, J. Environ. Sci., 32, 217–227, 10.1016/j.jes.2015.01.009, 2015.

Bushey, J. T., Nallana, A. G., Montesdeoca, M. R., and Driscoll, C. T.: Mercury dynamics of a northern hardwood canopy, Atmos. Environ., 42, 6905–6914, 10.1016/j.atmosenv.2008.05.043, 2008.

Castelle, S., Schäfer, J., Blanc, G., Dabrin, A., Lanceleur, L., and Masson, M.: Gaseous mercury at the air–water interface of a highly turbid estuary (Gironde Estuary, France), Mar. Chem., 117, 42–51, 10.1016/j.marchem.2009.01.005, 2009.

Castro, M. S., Moore, C., Sherwell, J., and Brooks, S. B.: Dry deposition of gaseous oxidized mercury in Western Maryland, Sci. Total Environ., 417-418, 232–240, 10.1016/j.scitotenv.2011.12.044, 2012.

Chen, L., Li, Y., Liu, C., Guo, L., and Wang, X.: Wet deposition of mercury in Qingdao, a coastal urban city in China: Concentrations, fluxes, and influencing factors, Atmos. Environ., 174, 204–213, 10.1016/j.atmosenv.2017.11.059, 2018.

Cheng, I., Zhang, L., and Mao, H.: Relative contributions of gaseous oxidized mercury and fine and coarse particle-bound mercury to mercury wet deposition at nine monitoring sites in North America, J. Geophys. Res. Atmos., 120, 8549–8562, 10.1002/2015jd023769, 2015.

Cheng , Z. L., Luo, Y., Zhang, T., and Duan, L.: Deposition of Sulfur， Nitrogen and Mercury in Two Typical Forest Ecosystems in Southern China, Environ. Sci., 2017.

Choi, H.-D., Sharac, T. J., and Holsen, T. M.: Mercury deposition in the Adirondacks: A comparison between precipitation and throughfall, Atmos. Environ., 42, 1818–1827, 10.1016/j.atmosenv.2007.11.036, 2008.

© Author(s) 2019. CC BY 4.0 License.

674 Ci, Z., Peng, F., Xue, X., and Zhang, X.: Air–surface exchange of gaseous mercury
675 over permafrost soil: an investigation at a high-altitude (4700 m a.s.l.) and
676 remote site in the central Qinghai–Tibet Plateau, Atmos. Chem. Phys., 16,
677 14741–14754, 10.5194/acp-16-14741-2016, 2016.
678 Ci, Z. J., Zhang, X. S., and Wang, Z. W.: Enhancing atmospheric mercury research in
679 China to improve the current understanding of the global mercury cycle: The
680 need for urgent and closely coordinated efforts, Environ. Sci. Technol., 46, 5636–
681 5642, 2012.
682 Connan, O., Maro, D., Hébert, D., Roupsard, P., Goujon, R., Letellier, B., and Le
683 Cavelier, S.: Wet and dry deposition of particles associated metals (Cd, Pb, Zn,
684 Ni, Hg) in a rural wetland site, Marais Vernier, France, Atmos. Environ., 67,
685 394–403, 10.1016/j.atmosenv.2012.11.029, 2013.
686 Converse, A. D., Riscassi, A. L., and Scanlon, T. M.: Seasonal variability in gaseous
687 mercury fluxes measured in a high-elevation meadow, Atmos. Environ., 44,
688 2176–2185, 10.1016/j.atmosenv.2010.03.024, 2010.
689 Converse, A. D., Riscassi, A. L., and Scanlon, T. M.: Seasonal contribution of dewfall
690 to mercury deposition determined using a micrometeorological technique and
691 dew chemistry, J. Geophys. Res. Atmos., 119(1), 284–292,
692 doi:10.1002/2013JD020491, 2014.
693 Dastoor, A. P., and Larocque, Y.: Global circulation of atmospheric mercury: a
694 modelling study, Atmos. Environ., 38, 147–161,
695 10.1016/j.atmosenv.2003.08.037, 2004.
696 Dutt, U., Nelson, P. F., Morrison, A. L., and Strezov, V.: Mercury wet deposition and
697 coal-fired power station contributions: An Australian study, Fuel Process.
698 Technol., 90, 1354–1359, 10.1016/j.fuproc.2009.06.019, 2009.
699 Eckley, C. S., Gustin, M., Lin, C. J., Li, X., and Miller, M. B.: The influence of
700 dynamic chamber design and operating parameters on calculated surface-to-air
701 mercury fluxes, Atmos. Environ., 44, 194–203, 10.1016/j.atmosenv.2009.10.013,
702 2010.
703 Eckley, C. S., Gustin, M., Marsik, F., and Miller, M. B.: Measurement of surface
704 mercury fluxes at active industrial gold mines in Nevada (USA), Sci. Total
705 Environ., 409, 514–522, 10.1016/j.scitotenv.2010.10.024, 2011.
706 Enrico, M., Roux, G. L., Marusczak, N., Heimburger, L. E., Claustres, A., Fu, X., Sun,
707 R., and Sonke, J. E.: Atmospheric mercury transfer to peat bogs dominated by

© Author(s) 2019. CC BY 4.0 License.

708 gaseous elemental mercury dry deposition, Environ. Sci. Technol., 50, 2405–
709 2412, 10.1021/acs.est.5b06058, 2016.
710 Fang, G.-C., Tsai, J.-H., Lin, Y.-H., and Chang, C.-Y.: Dry deposition of atmospheric
711 particle-bound mercury in the Middle Taiwan, Aerosol Air Qual. Res., 12, 1298–
712 1308, 10.4209/aaqr.2012.04.0093, 2012a.
713 Fang, G.-C., Lin, Y.-H., and Chang, C.-Y.: Use of mercury dry deposition samplers to
714 quantify dry deposition of particulate-bound mercury and reactive gaseous
715 mercury at a traffic sampling site, Environ. Forensics, 14, 182–186,
716 10.1080/15275922.2013.814177, 2013.
717 Fang, G. C., Zhang, L., and Huang, C. S.: Measurements of size-fractionated
718 concentration and bulk dry deposition of atmospheric particulate bound mercury,
719 Atmos. Environ., 61, 371–377, 10.1016/j.atmosenv.2012.07.052, 2012b.
720 Fisher, L. S., and Wolfe, M. H.: Examination of mercury inputs by throughfall and
721 litterfall in the Great Smoky Mountains National Park, Atmos. Environ., 47,
722 554–559, 10.1016/j.atmosenv.2011.10.017, 2012.
723 Fostier, A. H., Melendez-Perez, J. J., and Richter, L.: Litter mercury deposition in the
724 Amazonian rainforest, Environ. Pollut., 206, 605–610,
725 10.1016/j.envpol.2015.08.010, 2015.
726 Fragoso, C. P., Bernini, E., Araújo, B. F., Almeida, M. G. d., and Rezende, C. E. d.:
727 Mercury in litterfall and sediment using elemental and isotopic composition of
728 carbon and nitrogen in the mangrove of Southeastern Brazil, Estuarine Coastal
729 And Shelf Science, 202, 30–39, 10.1016/j.ecss.2017.12.005, 2018.
730 Fritsche, J., Obrist, D., Zeeman, M., Conen, F., Eugster, W., and Alewell, C.:
731 Elemental mercury fluxes over a sub-alpine grassland determined with two
732 micrometeorological methods, Atmos. Environ., 42, 2922–2933,
733 10.1016/j.atmosenv.2007.12.055, 2008a.
734 Fritsche, J., Wohlfahrt, G., Ammann, C., Zeeman, M., Hammerle, A., Obrist, D., and
735 Alewell, C.: Summertime elemental mercury exchange of temperate grasslands
736 on an ecosystem-scale, Atmos. Chem. Phys., 8, 10.5194/acp-8-7709-2008,
737 2008b.
738 Fu, X., Feng, X., Zhu, W., Zheng, W., Wang, S., and Lu, J. Y.: Total particulate and
739 reactive gaseous mercury in ambient air on the eastern slope of the Mt. Gongga
740 area, China, Appl. Geochem., 23, 408–418, 10.1016/j.apgeochem.2007.12.018,
741 2008.

© Author(s) 2019. CC BY 4.0 License.

742 Fu, X., Feng, X., Zhu, W., Rothenberg, S., Yao, H., and Zhang, H.: Elevated
743 atmospheric deposition and dynamics of mercury in a remote upland forest of
744 southwestern China, Environ. Pollut., 158, 2324–2333,
745 10.1016/j.envpol.2010.01.032, 2010a.
746 Fu, X. W., Feng, X., Dong, Z. Q., Yin, R. S., Wang, J. X., Yang, Z. R., and Zhang, H.:
747 Atmospheric gaseous elemental mercury (GEM) concentrations and mercury
748 depositions at a high-altitude mountain peak in south China, Atmos. Chem.
749 Phys., 10, 2425–2437, DOI 10.5194/acp-10-2425-2010, 2010b.
750 Fu, X., Feng, X., Sommar, J., and Wang, S.: A review of studies on atmospheric
751 mercury in China, Sci. Total Environ., 421–422, 73–81,
752 10.1016/j.scitotenv.2011.09.089, 2012.
753 Fu, X., Yang, X., Lang, X., Zhou, J., Zhang, H., Yu, B., Yan, H., Lin, C.-J., and Feng,
754 X.: Atmospheric wet and litterfall mercury deposition at urban and rural sites in
755 China, Atmos. Chem. Phys., 16, 11547–11562, 10.5194/acp-16-11547-2016,
756 2016.
757 Gerson, J. R., Driscoll, C. T., Demers, J. D., Sauer, A. K., Blackwell, B. D.,
758 Montesdeoca, M. R., Shanley, J. B., and Ross, D. S.: Deposition of mercury in
759 forests across a montane elevation gradient: Elevational and seasonal patterns in
760 methylmercury inputs and production, J. Geophys. Res. Biogeo., 122, 1922–
761 1939, 10.1002/2016jg003721, 2017.
762 Gichuki, S. W., and Mason, R. P.: Mercury and metals in South African precipitation,
763 Atmos. Environ., 79, 286–298, 10.1016/j.atmosenv.2013.04.009, 2013.
764 Gichuki, S. W., and Mason, R. P.: Wet and dry deposition of mercury in Bermuda,
765 Atmos. Environ., 87, 249–257, 10.1016/j.atmosenv.2014.01.025, 2014.
766 Gong, P., Wang, X. P., Xue, Y. G., Xu, B. Q., and Yao, T. D.: Mercury distribution in
767 the foliage and soil profiles of the Tibetan forest: processes and implications for
768 regional cycling, Environ. Pollut., 188, 94–101, 10.1016/j.envpol.2014.01.020,
769 2014.
770 Gratz, L. E., and Keeler, G. J.: Sources of mercury in precipitation to Underhill, VT,
771 Atmos. Environ., 45, 5440–5449, 10.1016/j.atmosenv.2011.07.001, 2011.
772 Guo, J., Kang, S., Huang, J., Zhang, Q., Rupakheti, M., Sun, S., Tripathee, L.,
773 Rupakheti, D., Panday, A. K., Sillanpaa, M., and Paudyal, R.: Characterizations
774 of atmospheric particulate-bound mercury in the Kathmandu Valley of Nepal,
775 South Asia, Sci. Total Environ., 579, 1240–1248,

© Author(s) 2019. CC BY 4.0 License.

776 10.1016/j.scitotenv.2016.11.110, 2017.
777 Guo, Y., Feng, X., Li, Z., He, T., Yan, H., Meng, B., Zhang, J., and Qiu, G.:
778 Distribution and wet deposition fluxes of total and methyl mercury in Wujiang
779 River Basin, Guizhou, China, Atmos. Environ., 42, 7096–7103,
780 10.1016/j.atmosenv.2008.06.006, 2008.
781 Gustin, M. S., Lindberg, S. E., and Weisberg, P. J.: An update on the natural sources
782 and sinks of atmospheric mercury, Appl. Geochem., 23, 482–493,
783 10.1016/j.apgeochem.2007.12.010, 2008.
784 Gustin, M. S., Weiss-Penzias, P. S., and Peterson, C.: Investigating sources of gaseous
785 oxidized mercury in dry deposition at three sites across Florida, USA, Atmos.
786 Chem. Phys., 12, 9201–9219, 10.5194/acp-12-9201-2012, 2012.
787 Gustin, M. S., Huang, J., Miller, M. B., Peterson, C., Jaffe, D. A., Ambrose, J., Finley,
788 B. D., Lyman, S. N., Call, K., Talbot, R., Feddersen, D., Mao, H., and Lindberg,
789 S. E.: Do we understand what the mercury speciation instruments are actually
790 measuring? Results of RAMIX, Environ. Sci. Technol., 47, 7295–7306,
791 10.1021/es3039104, 2013.
792 Gustin, M. S., Amos, H. M., Huang, J., Miller, M. B., and Heidecorn, K.: Measuring
793 and modeling mercury in the atmosphere: a critical review, Atmos. Chem. Phys.,
794 15, 5697–5713, 10.5194/acp-15-5697-2015, 2015.
795 Hall, N. L., Dvonch, J. T., Marsik, F. J., Barres, J. A., and Landis, M. S.: An artificial
796 turf-based surrogate surface collector for the direct measurement of atmospheric
797 mercury dry deposition, Int. J. Environ. Res. Public Health, 14,
798 10.3390/ijerph14020173, 2017.
799 Han, J.-S., Seo, Y.-S., Kim, M.-K., Holsen, T. M., and Yi, S.-M.: Total atmospheric
800 mercury deposition in forested areas in South Korea, Atmos. Chem. Phys., 16,
801 7653–7662, 10.5194/acp-16-7653-2016, 2016.
802 Hansen, A. M., and Gay, D. A.: Observations of mercury wet deposition in Mexico,
803 Environ. Sci. Pollut. Res. Int., 20, 8316–8325, 10.1007/s11356-013-2012-3,
804 2013.
805 Holmes, H. A., Pardyjak, E. R., Perry, K. D., and Abbott, M. L.: Gaseous dry
806 deposition of atmospheric mercury: A comparison of two surface resistance
807 models for deposition to semiarid vegetation, J. Geophys. Res., 116,
808 10.1029/2010jd015182, 2011.
809 Huang, J., Choi, H. D., Landis, M. S., and Holsen, T. M.: An application of passive

© Author(s) 2019. CC BY 4.0 License.

samplers to understand atmospheric mercury concentration and dry deposition spatial distributions, J Environ Monit, 14, 2976-2982, 10.1039/c2em30514c, 2012a.

Huang, J., Kang, S. C., Zhang, Q. G., Yan, H. Y., Guo, J. M., Jenkins, M. G., Zhang, G. S., and Wang, K.: Wet deposition of mercury at a remote site in the Tibetan Plateau: Concentrations, speciation, and fluxes, Atmos. Environ., 62, 540–550, 10.1016/j.atmosenv.2012.09.003, 2012b.

Huang, J., Kang, S., Wang, S., Wang, L., Zhang, Q., Guo, J., Wang, K., Zhang, G., and Tripathee, L.: Wet deposition of mercury at Lhasa, the capital city of Tibet, Sci. Total Environ., 447, 123–132, 10.1016/j.scitotenv.2013.01.003, 2013.

Huang, J., and Gustin, M. S.: Use of passive sampling methods and models to understand sources of mercury deposition to high elevation sites in the Western United States, Environ. Sci. Technol., 49, 432–441, 10.1021/es502836w, 2014.

Huang, J., Lyman, S. N., Hartman, J. S., and Gustin, M. S.: A review of passive sampling systems for ambient air mercury measurements, Environ. Sci.: Processes Impacts, 16, 374–392, 10.1039/c3em00501a, 2014.

Huang, J., and Gustin, M. S.: Uncertainties of gaseous oxidized mercury measurements using KCl-coated denuders, cation-exchange membranes, and nylon membranes: Humidity influences, Environ. Technol., 49, 6102–6108, 10.1021/acs.est.5b00098, 2015.

Huang, J., Kang, S., Zhang, Q., Guo, J., Sillanpaa, M., Wang, Y., Sun, S., Sun, X., and Tripathee, L.: Characterizations of wet mercury deposition on a remote high-elevation site in the southeastern Tibetan Plateau, Environ. Pollut., 206, 518–526, 10.1016/j.envpol.2015.07.024, 2015.

Huang, J., Kang, S., Guo, J., Zhang, Q., Cong, Z., Sillanpää, M., Zhang, G., Sun, S., and Tripathee, L.: Atmospheric particulate mercury in Lhasa city, Tibetan Plateau, Atmos. Environ., 142, 433–441, 10.1016/j.atmosenv.2016.08.021, 2016.

Huang, J. Y., Miller, M. B., Edgerton, E., and Gustin, M. S.: Deciphering potential chemical compounds of gaseous oxidized mercury in Florida, USA, Atmos. Chem. Phys., 17, 1689–1698, 10.5194/acp-17-1689-2017, 2017.

Juillerat, J. I., Ross, D. S., and Bank, M. S.: Mercury in litterfall and upper soil horizons in forested ecosystems in Vermont, USA, Environ. Toxicol. Chem., 31, 1720–1729, 10.1002/etc.1896, 2012.

Kamp, J., Skov, H., Jensen, B., and Sorensen, L. L.: Fluxes of gaseous elemental

© Author(s) 2019. CC BY 4.0 License.

mercury (GEM) in the High Arctic during atmospheric mercury depletion events (AMDEs), Atmos. Chem. Phys., 18, 6923–6938, 10.5194/acp-18-6923-2018, 2018.

Katata, G.: Fogwater deposition modeling for terrestrial ecosystems: A review of developments and measurements, J Geophys Res-Atmos, 119, Artn 2014jd021669
10.1002/2014jd021669, 2014.

Kim, M.-G., Lee, B.-K., and Kim, H.-J.: Cloud/fog water chemistry at a high elevation site in South Korea, J. Atmos. Chem., 55, 13–29, 10.1007/s10874-005-9004-8, 2006.

Lai, S. O., Huang, J., Hopke, P. K., and Holsen, T. M.: An evaluation of direct measurement techniques for mercury dry deposition, Sci. Total Environ., 409, 1320–1327, 10.1016/j.scitotenv.2010.12.032, 2011.

Larssen, T., de Wit, H. A., Wiker, M., and Halse, K.: Mercury budget of a small forested boreal catchment in southeast Norway, Sci. Total Environ., 404, 290–296, 10.1016/j.scitotenv.2008.03.013, 2008.

Lawson, S. T., Scherbatskoy, T. D., Malcolm, E. G., and Keeler, G. J.: Cloud water and throughfall deposition of mercury and trace elements in a high elevation spruce–fir forest at Mt. Mansfield, Vermont, J. Environ. Monit., 5, 578–583, 10.1039/b210125d, 2003.

Lin, C. J., Zhu, W., Li, X., Feng, X., Sommar, J., and Shang, L.: Novel dynamic flux chamber for measuring air-surface exchange of Hg(o) from soils, Environ. Sci. Technol., 46, 8910–8920, 10.1021/es3012386, 2012.

Lindberg, S. E., Bullock, R., Ebinghaus, R., Engstrom, D., Feng, X. B., Fitzgerald, W., Pirrone, N., Prestbo, E., and Seigneur, C.: A synthesis of progress and uncertainties in attributing the sources of mercury in deposition, Ambio, 36, 19–32, 2007.

Lombard, M. A. S., Bryce, J. G., Mao, H., and Talbot, R.: Mercury deposition in Southern New Hampshire, 2006–2009, Atmos. Chem. Phys., 11, 7657–7668, 10.5194/acp-11-7657-2011, 2011.

Lu, A., and Liu, H.: Study on the time distribution characteristics and source of wet deposition mercury in weinan city, Journal of Arid Land Resources and Environment, 2018.

© Author(s) 2019. CC BY 4.0 License.

877 Luo, Y., Duan, L., Wang, L., Xu, G., Wang, S., and Hao, J.: Mercury concentrations in
878 forest soils and stream waters in northeast and south China, Sci. Total Environ.,
879 496, 714–720, 10.1016/j.scitotenv.2014.07.036, 2014.
880 Luo, Y., Duan, L., Driscoll, C. T., Xu, G. Y., Shao, M. S., Taylor, M., Wang, S. X., and
881 Hao, J. M.: Foliage/atmosphere exchange of mercury in a subtropical coniferous
882 forest in south China, J. Geophys. Res. Biogeo., 121, 2006–2016,
883 10.1002/2016jg003388, 2016.
884 Lyman, S. N., Gustin, M. S., Prestbo, E. M., and Marsik, F. J.: Estimation of dry
885 deposition of atmospheric mercury in Nevada by direct and indirect methods,
886 Environ. Sci. Technol., 41, 1970–1976, 2007.
887 Lyman, S. N., Gustin, M. S., Prestbo, E. M., Kilner, P. I., Edgerton, E., and Hartsell,
888 B.: Testing and application of surrogate surfaces for understanding potential
889 gaseous oxidized mercury dry deposition, Environ. Sci. Technol., 43, 6235–6241,
890 2009.
891 Lyman, S. N., Jaffe, D. A., and Gustin, M. S.: Release of mercury halides from KCl
892 denuders in the presence of ozone, Atmos. Chem. Phys., 10, 8197–8204,
893 10.5194/acp-10-8197-2010, 2010.
894 Lynam, M., Dvonch, J. T., Barres, J., and Percy, K.: Atmospheric wet deposition of
895 mercury to the Athabasca Oil Sands Region, Alberta, Canada, Air Qual. Atmos.
896 Health, 11, 83–93, 10.1007/s11869-017-0524-6, 2017.
897 Lynam, M. M., Dvonch, J. T., Hall, N. L., Morishita, M., and Barres, J. A.: Spatial
898 patterns in wet and dry deposition of atmospheric mercury and trace elements in
899 central Illinois, USA, Environ. Sci. Pollut. Res. Int., 21, 4032–4043,
900 10.1007/s11356-013-2011-4, 2014.
901 Ma, M., Wang, D., Du, H., Sun, T., Zhao, Z., and Wei, S.: Atmospheric mercury
902 deposition and its contribution of the regional atmospheric transport to mercury
903 pollution at a national forest nature reserve, southwest China, Environ. Sci.
904 Pollut. Res. Int., 22, 20007–20018, 10.1007/s11356-015-5152-9, 2015.
905 Ma, M., Wang, D., Du, H., Sun, T., Zhao, Z., Wang, Y., and Wei, S.: Mercury
906 dynamics and mass balance in a subtropical forest, southwestern China, Atmos.
907 Chem. Phys., 16, 4529–4537, 10.5194/acp-16-4529-2016, 2016.
908 Ma, M., Sun, T., Du, H., and Wang, D.: A Two-Year Study on Mercury Fluxes from
909 the Soil under Different Vegetation Cover in a Subtropical Region, South China,
910 Atmosphere, 9, 30, 10.3390/atmos9010030, 2018.

© Author(s) 2019. CC BY 4.0 License.

911 Malcolm, E. G., Keeler, G. J., Lawson, S. T., and Sherbatskoy, T. D.: Mercury and
912 trace elements in cloud water and precipitation collected on Mt. Mansfield,
913 Vermont, J. Environ. Monit., 5, 584, 10.1039/b210124f, 2003.
914 Marsik, F. J., Keeler, G. J., and Landis, M. S.: The dry-deposition of speciated
915 mercury to the Florida Everglades: Measurements and modeling, Atmos.
916 Environ., 41, 136–149, 10.1016/j.atmosenv.2006.07.032, 2007.
917 Marumoto, K., and Matsuyama, A.: Mercury speciation in wet deposition samples
918 collected from a coastal area of Minamata Bay, Atmos. Environ., 86, 220–227,
919 10.1016/j.atmosenv.2013.12.011, 2014.
920 McClure, C. D., Jaffe, D. A., and Edgerton, E. S.: Evaluation of the KCl denuder
921 method for gaseous oxidized mercury using HgBr2 at an in-service AMNet site,
922 Environ. Sci. Technol., 48, 11437–11444, 10.1021/es502545k, 2014.
923 Miller, M. B., Gustin, M. S., and Eckley, C. S.: Measurement and scaling of air-
924 surface mercury exchange from substrates in the vicinity of two Nevada gold
925 mines, Sci. Total Environ., 409, 3879–3886, 10.1016/j.scitotenv.2011.05.040,
926 2011.
927 Navrátil, T., Shanley, J., Rohovec, J., Hojdová, M., Penížek, V., and Buchtová, J.:
928 Distribution and pools of mercury in Czech forest soils, Water Air and Soil
929 Pollution, 225, 10.1007/s11270-013-1829-1, 2014.
930 Nguyen, D. L., Kim, J. Y., Shim, S. G., Ghim, Y. S., and Zhang, X. S.: Shipboard and
931 ground measurements of atmospheric particulate mercury and total mercury in
932 precipitation over the Yellow Sea region, Environ. Pollut., 219, 262–274,
933 10.1016/j.envpol.2016.10.020, 2016.
934 Obrist, D., Conen, F., Vogt, R., Siegwolf, R., and Alewell, C.: Estimation of Hg0
935 exchange between ecosystems and the atmosphere using 222Rn and Hg0
936 concentration changes in the stable nocturnal boundary layer, Atmos. Environ.,
937 40, 856–866, 10.1016/j.atmosenv.2005.10.012, 2006.
938 Obrist, D., Johnson, D. W., and Lindberg, S. E.: Mercury concentrations and pools in
939 four Sierra Nevada forest sites, and relationships to organic carbon and nitrogen,
940 Biogeosciences, 6, 765–777, DOI 10.5194/bg-6-765-2009, 2009.
941 Obrist, D., Johnson, D. W., and Edmonds, R. L.: Effects of vegetation type on
942 mercury concentrations and pools in two adjacent coniferous and deciduous
943 forests, Journal of Plant Nutrition and Soil Science, 175, 68–77,
944 10.1002/jpln.201000415, 2012.

© Author(s) 2019. CC BY 4.0 License.

945 Obrist, D., Agnan, Y., Jiskra, M., Olson, C. L., Colegrove, D. P., Hueber, J., Moore, C.
946 W., Sonke, J. E., and Helmig, D.: Tundra uptake of atmospheric elemental
947 mercury drives Arctic mercury pollution, Nat. Clim. Change, 547, 201–204,
948 10.1038/nature22997, 2017.
949 Obrist, D., Kirk, J. L., Zhang, L., Sunderland, E. M., Jiskra, M., and Selin, N. E.: A
950 review of global environmental mercury processes in response to human and
951 natural perturbations: Changes of emissions, climate, and land use, Ambio, 47,
952 116–140, 10.1007/s13280-017-1004-9, 2018.
953 Osterwalder, S., Fritsche, J., Alewell, C., Schmutz, M., Nilsson, M. B., Jocher, G.,
954 Sommar, J., Rinne, J., and Bishop, K.: A dual-inlet, single detector relaxed eddy
955 accumulation system for long-term measurement of mercury flux, Atmos. Meas.
956 Tech., 9, 509–524, 10.5194/amt-9-509-2016, 2016.
957 Osterwalder, S., Sommar, J., Åkerblom, S., Jocher, G., Fritsche, J., Nilsson, M. B.,
958 Bishop, K., and Alewell, C.: Comparative study of elemental mercury flux
959 measurement techniques over a Fennoscandian boreal peatland, Atmos. Environ.,
960 172, 16–25, 10.1016/j.atmosenv.2017.10.025, 2018.
961 Peterson, C., Alishahi, M., and Gustin, M. S.: Testing the use of passive sampling
962 systems for understanding air mercury concentrations and dry deposition across
963 Florida, USA, Sci. Total Environ., 424, 297–307,
964 10.1016/j.scitotenv.2012.02.031, 2012.
965 Pierce, A. M., Moore, C. W., Wohlfahrt, G., Hortnagl, L., Kljun, N., and Obrist, D.:
966 Eddy covariance flux measurements of gaseous elemental mercury using cavity
967 ring-down spectroscopy, Environ. Sci. Technol., 49, 1559–1568,
968 10.1021/es505080z, 2015.
969 Prestbo, E. M., and Gay, D. A.: Wet deposition of mercury in the US and Canada,
970 1996-2005: Results and analysis of the NADP mercury deposition network
971 (MDN), Atmos. Environ., 43, 4223–4233, 10.1016/j.atmosenv.2009.05.028,
972 2009.
973 Qin, C., Wang, Y., Peng, Y., and Wang, D.: Four-year record of mercury wet
974 deposition in one typical industrial city in southwest China, Atmos. Environ.,
975 142, 442–451, 10.1016/j.atmosenv.2016.08.016, 2016.
976 Richardson, J. B., and Friedland, A. J.: Mercury in coniferous and deciduous upland
977 forests in Northern New England, USA: implications from climate change,
978 Biogeosciences, 12, 11463–11498, 10.5194/bgd-12-11463-2015, 2015.

© Author(s) 2019. CC BY 4.0 License.

979 Risch, M., and Kenski, D.: Spatial Patterns and Temporal Changes in Atmospheric-
980 Mercury Deposition for the Midwestern USA, 2001–2016, Atmosphere, 9, 29,
981 10.3390/atmos9010029, 2018.
982 Risch, M. R., DeWild, J. F., Gay, D. A., Zhang, L., Boyer, E. W., and Krabbenhoft, D.
983 P.: Atmospheric mercury deposition to forests in the eastern USA, Environ.
984 Pollut., 228, 8–18, 10.1016/j.envpol.2017.05.004, 2017.
985 Sakata, M., and Marumoto, K.: Wet and dry deposition fluxes of mercury in Japan,
986 Atmos. Environ., 39, 3139–3146, 10.1016/j.atmosenv.2005.01.049, 2005.
987 Sather, M. E., Mukerjee, S., Smith, L., Mathew, J., Jackson, C., Callison, R., Scrapper,
988 L., Hathcoat, A., Adam, J., Keese, D., Ketcher, P., Brunette, R., Karlstrom, J.,
989 and Van der Jagt, G.: Gaseous oxidized mercury dry deposition measurements in
990 the Four Corners area and Eastern Oklahoma, U.S.A, Atmos. Pollut. Res., 4,
991 168–180, 10.5094/apr.2013.017, 2013.
992 Sather, M. E., Mukerjee, S., Allen, K. L., Smith, L., Mathew, J., Jackson, C., Callison,
993 R., Scrapper, L., Hathcoat, A., Adam, J., Keese, D., Ketcher, P., Brunette, R.,
994 Karlstrom, J., and Van der Jagt, G.: Gaseous oxidized mercury dry deposition
995 measurements in the southwestern USA: A comparison between Texas, Eastern
996 Oklahoma, and the Four Corners Area, Sci. World J., 2014, 580723,
997 10.1155/2014/580723, 2014.
998 Schroeder, W. H., and Munthe, J.: Atmospheric mercury - An overview, Atmos.
999 Environ., 32, 809–822, 1998.
1000 Schwab, J. J., Casson, P., Brandt, R., Husain, L., Dutkewicz, V., Wolfe, D., Demerjian,
1001 K. L., Civerolo, K. L., Rattigan, O. V., Felton, H. D., and Dukett, J. E.:
1002 Atmospheric chemistry measurements at Whiteface Mountain, NY: Cloud water
1003 chemistry, precipitation chemistry, and particulate matter, Aerosol Air Qual. Res.,
1004 16, 841–854, 10.4209/aaqr.2015.05.0344, 2016.
1005 Seinfeld, J. H., and Pandis, S. N.: Atmospheric Chemistry and Physics: From Air
1006 Pollution to Climate Change (3rd Edition), Wiley, 2016.
1007 Seo, Y.-S., Han, Y.-J., Choi, H.-D., Holsen, T. M., and Yi, S.-M.: Characteristics of
1008 total mercury (TM) wet deposition: Scavenging of atmospheric mercury species,
1009 Atmos. Environ., 49, 69–76, 10.1016/j.atmosenv.2011.12.031, 2012.
1010 Sheu, G.-R., and Lin, N.-H.: Mercury in cloud water collected on Mt. Bamboo in
1011 northern Taiwan during the northeast monsoon season, Atmos. Environ., 45,
1012 4454–4462, 10.1016/j.atmosenv.2011.05.036, 2011.

© Author(s) 2019. CC BY 4.0 License.

1013 Sheu, G.-R., and Lin, N.-H.: Characterizations of wet mercury deposition to a remote
1014 islet (Pengjiayu) in the subtropical Northwest Pacific Ocean, Atmos. Environ.,
1015 77, 474–481, 10.1016/j.atmosenv.2013.05.038, 2013.
1016 Siudek, P., Kurzyca, I., and Siepak, J.: Atmospheric deposition of mercury in central
1017 Poland: Sources and seasonal trends, Atmos. Res., 170, 14–22,
1018 10.1016/j.atmosres.2015.11.004, 2016.
1019 Sommar, J., Zhu, W., Lin, C.-J., and Feng, X.: Field approaches to measure Hg
1020 exchange between natural surfaces and the atmosphere—A review, Crit. Rev.
1021 Environ. Sci. Technol., 43, 1657–1739, 10.1080/10643389.2012.671733, 2013a.
1022 Sommar, J., Zhu, W., Shang, L., Feng, X., and Lin, C.-J.: A whole-air relaxed eddy
1023 accumulation measurement system for sampling vertical vapour exchange of
1024 elemental mercury, Tellus B Chem. Phys. Meteorol., 65, 19940,
1025 10.3402/tellusb.v65i0.19940, 2013b.
1026 Sommar, J., Zhu, W., Shang, L., Lin, C.-J., and Feng, X.: Seasonal variations in
1027 metallic mercury (Hg0) vapor exchange over biannual wheat–corn rotation
1028 cropland in the North China Plain, Biogeosciences, 13, 2029–2049, 10.5194/bg-
1029 13-2029-2016, 2016.
1030 Sprovieri, F., Pirrone, N., Bencardino, M., D'Amore, F., Angot, H., Barbante, C.,
1031 Brunke, E. G., Arcega-Cabrera, F., Cairns, W., Comero, S., Dieguez, M. D.,
1032 Dommergue, A., Ebinghaus, R., Feng, X. B., Fu, X. W., Garcia, P. E., Gawlik, B.
1033 M., Hagestrom, U., Hansson, K., Horvat, M., Kotnik, J., Labuschagne, C.,
1034 Magand, O., Martin, L., Mashyanov, N., Mkololo, T., Munthe, J., Obolkin, V.,
1035 Islas, M. R., Sena, F., Somerset, V., Spandow, P., Varde, M., Walters, C.,
1036 Wangberg, I., Weigelt, A., Yang, X., and Zhang, H.: Five-year records of mercury
1037 wet deposition flux at GMOS sites in the Northern and Southern hemispheres,
1038 Atmos. Chem. Phys., 17, 2689–2708, 10.5194/acp-17-2689-2017, 2017.
1039 Stankwitz, C., Kaste, J. M., and Friedland, A. J.: Threshold increases in soil lead and
1040 mercury from tropospheric deposition across an elevational gradient, Environ.
1041 Sci. Technol., 46, 8061–8068, 10.1021/es204208w, 2012.
1042 Teixeira, D. C., Montezuma, R. C., Oliveira, R. R., and Silva-Filho, E. V.: Litterfall
1043 mercury deposition in Atlantic forest ecosystem from SE-Brazil, Environ. Pollut.,
1044 164, 11–15, 10.1016/j.envpol.2011.10.032, 2012.
1045 Teixeira, D. C., Lacerda, L. D., and Silva-Filho, E. V.: Mercury sequestration by
1046 rainforests: The influence of microclimate and different successional stages,

© Author(s) 2019. CC BY 4.0 License.

Chemosphere, 168, 1186–1193, 10.1016/j.chemosphere.2016.10.081, 2017.

Torseth, K., Aas, W., Breivik, K., Fjaeraa, A. M., Fiebig, M., Hjellbrekke, A. G., Myhre, C. L., Solberg, S., and Yttri, K. E.: Introduction to the European Monitoring and Evaluation Programme (EMEP) and observed atmospheric composition change during 1972-2009, Atmos. Chem. Phys., 12, 5447–5481, 10.5194/acp-12-5447-2012, 2012.

Wan, Q., Feng, X., Lu, J., Zheng, W., Song, X., Li, P., Han, S., and Xu, H.: Atmospheric mercury in Changbai Mountain area, northeastern China II. The distribution of reactive gaseous mercury and particulate mercury and mercury deposition fluxes, Environ. Res., 109, 721–727, 10.1016/j.envres.2009.05.006, 2009.

Wang, X., Lin, C. J., and Feng, X.: Sensitivity analysis of an updated bidirectional air–surface exchange model for elemental mercury vapor, Atmos. Chem. Phys., 14, 6273–6287, 10.5194/acp-14-6273-2014, 2014.

Wang, X., Bao, Z., Lin, C. J., Yuan, W., and Feng, X.: Assessment of global mercury deposition through litterfall, Environ. Sci. Technol., 50, 8548–8557, 10.1021/acs.est.5b06351, 2016a.

Wang, X., Lin, C.-J., Lu, Z., Zhang, H., Zhang, Y., and Feng, X.: Enhanced accumulation and storage of mercury on subtropical evergreen forest floor: Implications on mercury budget in global forest ecosystems, J. Geophys. Res. Biogeo., 121, 2096–2109, 10.1002/2016jg003446, 2016b.

Wang, Z., Zhang, X., Xiao, J., Ci, Z., and Yu, P.: Mercury fluxes and pools in three subtropical forested catchments, southwest China, Environ. Pollut., 157, 801–808, 10.1016/j.envpol.2008.11.018, 2009.

Weiss-Penzias, P., Fernandez, D., Moranville, R., and Saltikov, C.: A low cost system for detecting fog events and triggering an active fog water collector, Aerosol Air Qual. Res., 18, 214–233, 10.4209/aaqr.2016.11.0508, 2018.

Weiss-Penzias, P. S., Gustin, M. S., and Lyman, S. N.: Sources of gaseous oxidized mercury and mercury dry deposition at two southeastern U.S. sites, Atmos. Environ., 45, 4569–4579, 10.1016/j.atmosenv.2011.05.069, 2011.

Weiss-Penzias, P. S., Gay, D. A., Brigham, M. E., Parsons, M. T., Gustin, M. S., and Ter Schure, A.: Trends in mercury wet deposition and mercury air concentrations across the U.S. and Canada, Sci. Total Environ., 568, 546–556, 10.1016/j.scitotenv.2016.01.061, 2016.

© Author(s) 2019. CC BY 4.0 License.

1081 Wetang'ula: Preliminary assessment of total mercury in bulk precipitation around
1082 Olkaria Area, Kenya, Journal of Environmental Science and Engineering, 1585–
1083 1595, 2011.
1084 Wright, G., Gustin, M. S., Weiss-Penzias, P., and Miller, M. B.: Investigation of
1085 mercury deposition and potential sources at six sites from the Pacific Coast to the
1086 Great Basin, USA, Sci. Total Environ., 470-471, 1099–1113,
1087 10.1016/j.scitotenv.2013.10.071, 2014.
1088 Wright, L. P., and Zhang, L.: An approach estimating bidirectional air-surface
1089 exchange for gaseous elemental mercury at AMNet sites, J. Adv. Model. Earth
1090 Sy., 7, 35–49, 10.1002/2014ms000367, 2015.
1091 Wright, L. P., Zhang, L. M., and Marsik, F. J.: Overview of mercury dry deposition,
1092 litterfall, and throughfall studies, Atmos. Chem. Phys., 16, 13399–13416,
1093 10.5194/acp-16-13399-2016, 2016.
1094 Xu, L., Chen, J., Yang, L., Yin, L., Yu, J., Qiu, T., and Hong, Y.: Characteristics of
1095 total and methyl mercury in wet deposition in a coastal city, Xiamen, China:
1096 Concentrations, fluxes and influencing factors on Hg distribution in precipitation,
1097 Atmos. Environ., 99, 10–16, 10.1016/j.atmosenv.2014.09.054, 2014.
1098 Yu, Q., Luo, Y., Wang, S. X., Wang, Z. Q., Hao, J. M., and Duan, L.: Gaseous
1099 elemental mercury (GEM) fluxes over canopy of two typical subtropical forests
1100 in south China, Atmos. Chem. Phys., 18, 495–509, 10.5194/acp-18-495-2018,
1101 2018.
1102 Zhang, L., Brook, J. R., and Vet, R.: A revised parameterization for gaseous dry
1103 deposition in air-quality models, Atmos. Chem. Phys., 3, 2067–2082, DOI
1104 10.5194/acp-3-2067-2003, 2003.
1105 Zhang, L., Blanchard, P., Gay, D. A., Prestbo, E. M., Risch, M. R., Johnson, D.,
1106 Narayan, J., Zsolway, R., Holsen, T. M., Miller, E. K., Castro, M. S., Graydon, J.
1107 A., St Louis, V. L., and Dalziel, J.: Estimation of speciated and total mercury dry
1108 deposition at monitoring locations in eastern and central North America, Atmos.
1109 Chem. Phys., 12, 4327–4340, 10.5194/acp-12-4327-2012, 2012.
1110 Zhang, L., and He, Z.: Technical Note: An empirical algorithm estimating dry
1111 deposition velocity of fine, coarse and giant particles, Atmos. Chem. Phys., 14,
1112 3729–3737, 10.5194/acp-14-3729-2014, 2014.
1113 Zhang, L., Wang, S. X., Wu, Q. R., Wang, F. Y., Lin, C.-J., Zhang, L. M., Hui, M. L.,
1114 Yang, M., Su, H. T., and Hao, J. M.: Mercury transformation and speciation in

© Author(s) 2019. CC BY 4.0 License.

flue gases from anthropogenic emission sources: a critical review, Atmos. Chem. Phys., 16, 2417–2433, 10.5194/acp-16-2417-2016, 2016a.

Zhang, L., Wu, Z., Cheng, I., Wright, L. P., Olson, M. L., Gay, D. A., Risch, M. R., Brooks, S., Castro, M. S., Conley, G. D., Edgerton, E. S., Holsen, T. M., Luke, W., Tordon, R., and Weiss-Penzias, P.: The estimated six-year mercury dry deposition across North America, Environ. Sci. Technol., 50, 12864–12873, 10.1021/acs.est.6b04276, 2016b.

Zhang, L. M., Gong, S. L., Padro, J., and Barrie, L.: A size-segregated particle dry deposition scheme for an atmospheric aerosol module, Atmos. Environ., 35, 549–560, Doi 10.1016/S1352-2310(00)00326-5, 2001.

Zhang, L. M., Moran, M. D., Makar, P. A., Brook, J. R., and Gong, S. L.: Modelling gaseous dry deposition in AURAMS: A unified regional air-quality modelling system, Atmos. Environ., 36, 537–560, Doi 10.1016/S1352-2310(01)00447-2, 2002.

Zhang, L. M., Wright, L. P., and Blanchard, P.: A review of current knowledge concerning dry deposition of atmospheric mercury, Atmos. Environ., 43, 5853–5864, 10.1016/j.atmosenv.2009.08.019, 2009.

Zhang, Y., Liu, R., Wang, Y., Cui, X., and Qi, J.: Change characteristic of atmospheric particulate mercury during dust weather of spring in Qingdao, China, Atmos. Environ., 102, 376–383, 10.1016/j.atmosenv.2014.12.005, 2015.

Zhao, Z., Wang, D., Wang, Y., Mu, Z., and Zhu, J.: Wet deposition flux and runoff output flux of mercury in a typical small agricultural watershed in Three Gorges Reservoir areas, Environ. Sci. Pollut. Res. Int., 22, 5538–5551, 10.1007/s11356-014-3701-2, 2015.

Zhou, J., Wang, Z., Sun, T., Zhang, H., and Zhang, X.: Mercury in terrestrial forested systems with highly elevated mercury deposition in southwestern China: The risk to insects and potential release from wildfires, Environ. Pollut., 212, 188–196, 10.1016/j.envpol.2016.01.003, 2016.

Zhou, J., Wang, Z., Zhang, X., and Gao, Y.: Mercury concentrations and pools in four adjacent coniferous and deciduous upland forests in Beijing, China, J. Geophys. Res. Biogeo., 122, 1260–1274, 10.1002/2017jg003776, 2017.

Zhu, J., Wang, T., Talbot, R., Mao, H., Yang, X., Fu, C., Sun, J., Zhuang, B., Li, S., Han, Y., and Xie, M.: Characteristics of atmospheric mercury deposition and size-fractionated particulate mercury in urban Nanjing, China, Atmos. Chem.

© Author(s) 2019. CC BY 4.0 License.

Phys., 14, 2233–2244, 10.5194/acp-14-2233-2014, 2014.

Zhu, W., Sommar, J., Lin, C. J., and Feng, X.: Mercury vapor air–surface exchange measured by collocated micrometeorological and enclosure methods – Part II: Bias and uncertainty analysis, Atmos. Chem. Phys., 15, 5359–5376, 10.5194/acp-15-5359-2015, 2015a.

Zhu, W., Sommar, J., Lin, C. J., and Feng, X.: Mercury vapor air–surface exchange measured by collocated micrometeorological and enclosure methods – Part I: Data comparability and method characteristics, Atmos. Chem. Phys., 15, 685–702, 10.5194/acp-15-685-2015, 2015b.

Zhu, W., Lin, C.-J., Wang, X., Sommar, J., Fu, X., and Feng, X.: Global observations and modeling of atmosphere–surface exchange of elemental mercury: A critical review, Atmos. Chem. Phys., 16, 4451–4480, 10.5194/acp-16-4451-2016, 2016.

© Author(s) 2019. CC BY 4.0 License.

Figure Captions

Figure 1. Global distribution of the Hg wet deposition flux (μg m^{-2} yr^{-1}).

Figure 2. Relationships between the annual precipitation and the Hg wet deposition flux for different regions worldwide.

Figure 3. Global distribution of the (a) GOM, (b) PBM, and (c) GEM dry deposition fluxes (μg m^{-2} yr^{-1}).

Figure 4. Relationship between the elevation and the GOM dry deposition flux.

Figure 5. Comparison between the GOM dry deposition fluxes from direct observations and model simulations. The numbers in brackets stand for the numbers of samples.

Figure 6. Total Hg wet deposition fluxes (blue columns with black bars as standard deviations) and precipitation levels (orange dots) for (a) different terrestrial surface types and (b) different forest types. The numbers in brackets stand for the numbers of samples. DB stands for deciduous broadleaf forests, DN stands for deciduous needle leaf forests, EB stands for evergreen broadleaf forests, and EN stands for evergreen needle leaf forests.

Figure 7. Dry deposition fluxes of (a) GOM, (b) PBM and (c) GEM for different terrestrial surface types. The numbers in brackets stand for the numbers of samples.

Figure 8. Litterfall Hg deposition fluxes (blue columns with black bars as standard deviations) and Hg concentrations in litterfall (orange dots) for different terrestrial surface types. The numbers in brackets stand for the numbers of samples. DB stands for deciduous broadleaf forests, DN stands for deciduous needle leaf forests, EB stands for evergreen broadleaf forests, and EN stands for evergreen needle leaf forests.

Atmos. Chem. Phys. Discuss., https://doi.org/10.5194/acp-2019-347
Manuscript under review for journal Atmos. Chem. Phys.
Discussion started: 13 May 2019
© Author(s) 2019. CC BY 4.0 License.

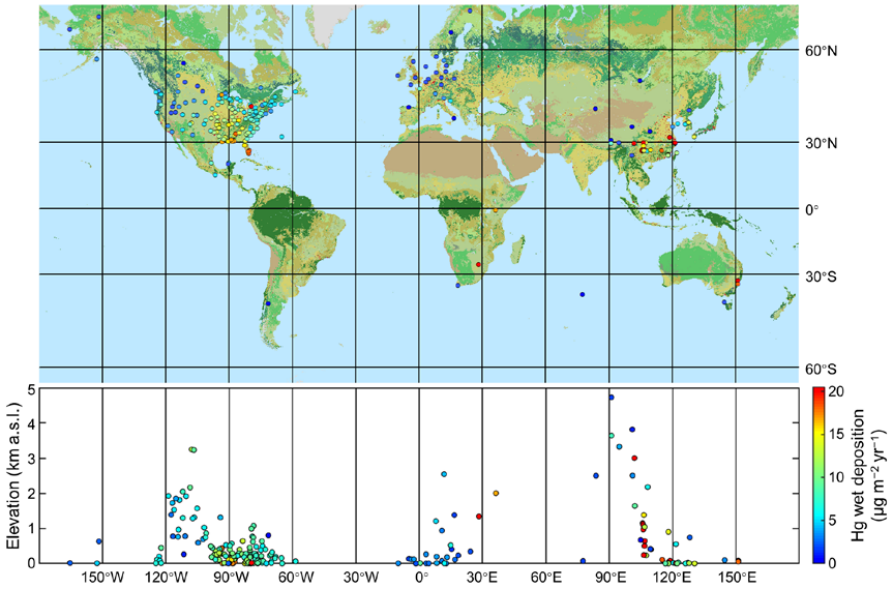

Figure 1. Global distribution of the Hg wet deposition flux (μg m^{-2} yr^{-1}).

© Author(s) 2019. CC BY 4.0 License.

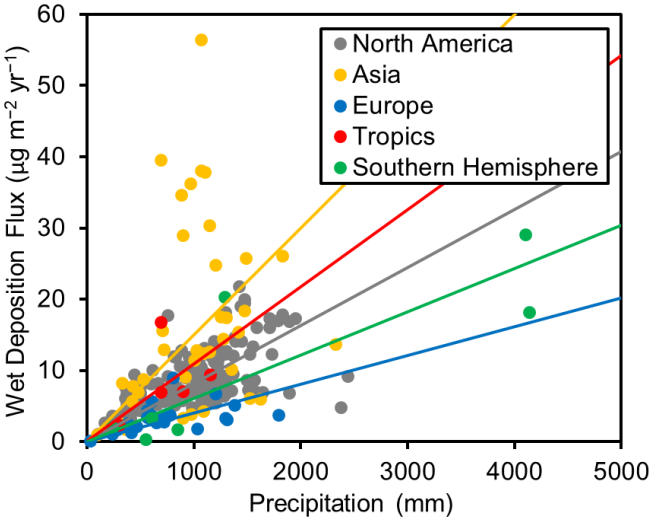

Figure 2. Relationships between the annual precipitation and the Hg wet deposition flux for different regions worldwide.

Atmos. Chem. Phys. Discuss., https://doi.org/10.5194/acp-2019-347
Manuscript under review for journal Atmos. Chem. Phys.
Discussion started: 13 May 2019
© Author(s) 2019. CC BY 4.0 License.

Atmospheric Chemistry and Physics Discussions

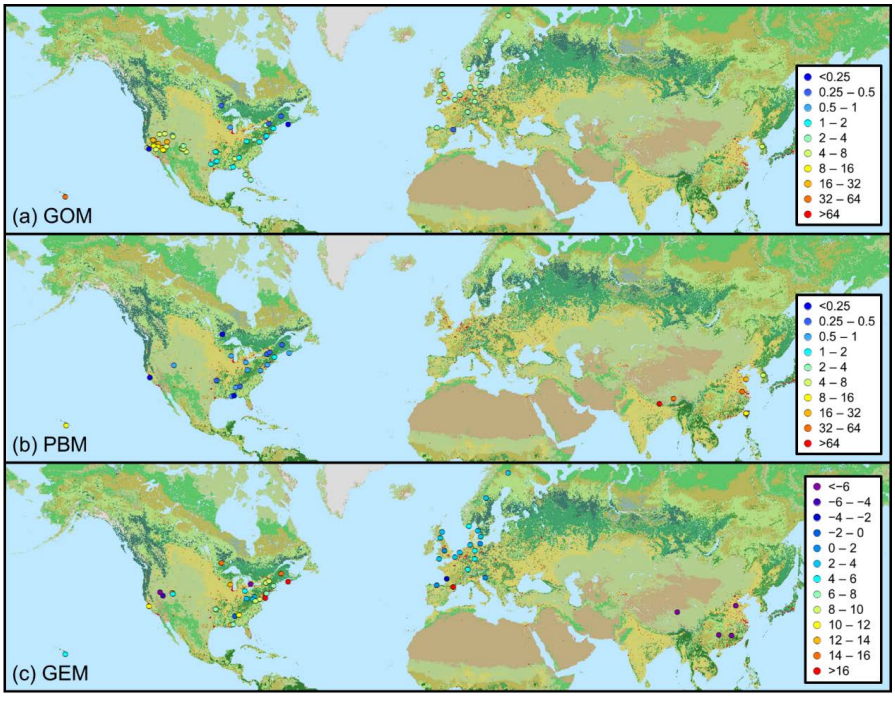

Figure 3. Global distribution of the (a) GOM, (b) PBM, and (c) GEM dry deposition fluxes (μg m^{-2} yr^{-1}).

Atmos. Chem. Phys. Discuss., https://doi.org/10.5194/acp-2019-347
Manuscript under review for journal Atmos. Chem. Phys.
Discussion started: 13 May 2019
© Author(s) 2019. CC BY 4.0 License.

Atmospheric Chemistry and Physics Discussions

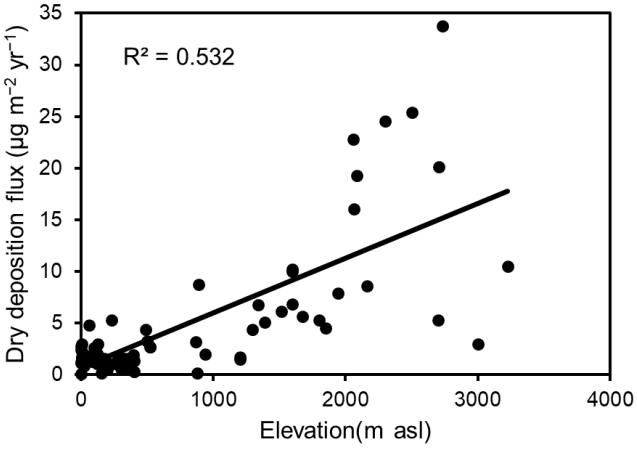

1197

1198 **Figure 4.** Relationship between the elevation and the GOM dry deposition flux.

1199

Atmos. Chem. Phys. Discuss., https://doi.org/10.5194/acp-2019-347
Manuscript under review for journal Atmos. Chem. Phys.
Discussion started: 13 May 2019
© Author(s) 2019. CC BY 4.0 License.

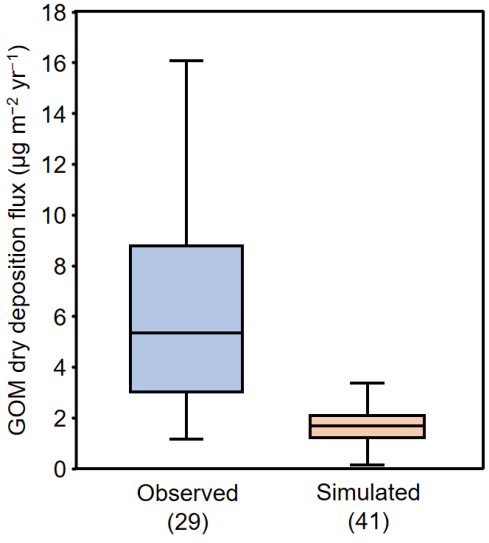

Figure 5. Comparison between the GOM dry deposition fluxes from direct observations and model simulations. The numbers in brackets stand for the numbers of samples.

Atmos. Chem. Phys. Discuss., https://doi.org/10.5194/acp-2019-347
Manuscript under review for journal Atmos. Chem. Phys.
Discussion started: 13 May 2019
© Author(s) 2019. CC BY 4.0 License.

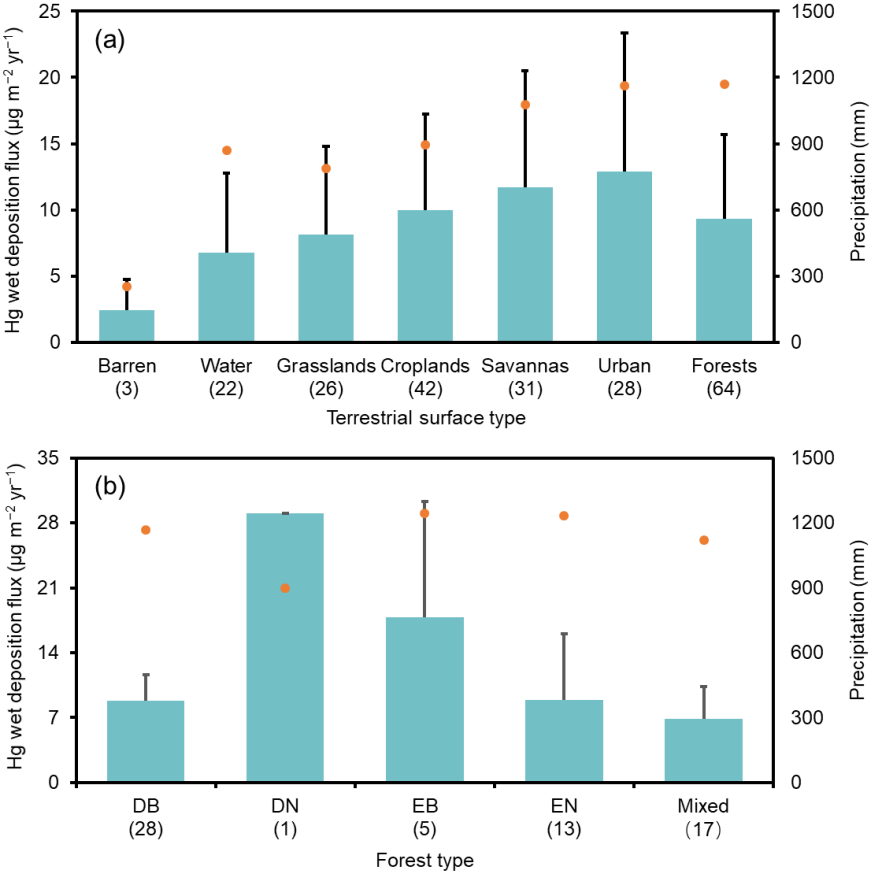

Figure 6. Total Hg wet deposition fluxes (blue columns with black bars as standard deviations) and precipitation levels (orange dots) for (a) different terrestrial surface types and (b) different forest types. The numbers in brackets stand for the numbers of samples. DB stands for deciduous broadleaf forests, DN stands for deciduous needle leaf forests, EB stands for evergreen broadleaf forests, and EN stands for evergreen needle leaf forests.

Atmos. Chem. Phys. Discuss., https://doi.org/10.5194/acp-2019-347
Manuscript under review for journal Atmos. Chem. Phys.
Discussion started: 13 May 2019
© Author(s) 2019. CC BY 4.0 License.

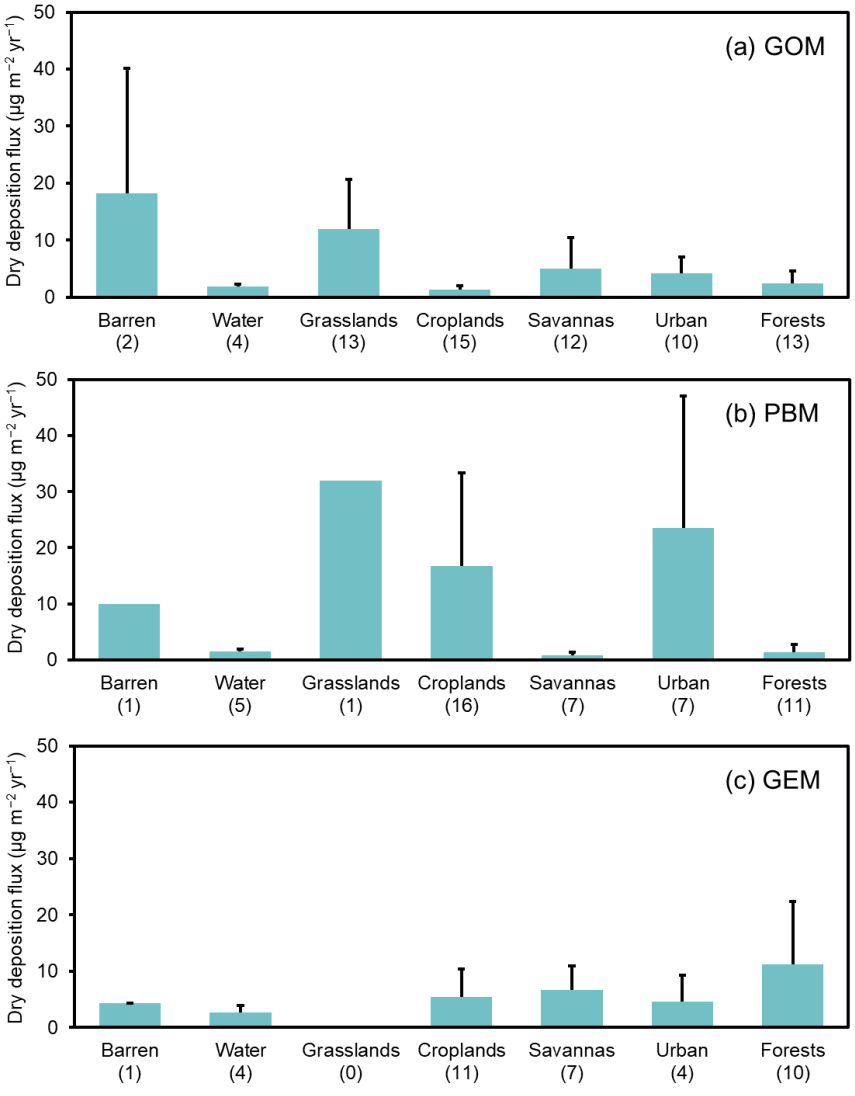

Figure 7. Dry deposition fluxes of (a) GOM, (b) PBM and (c) GEM for different terrestrial surface types. The numbers in brackets stand for the numbers of samples.

Atmos. Chem. Phys. Discuss., https://doi.org/10.5194/acp-2019-347
Manuscript under review for journal Atmos. Chem. Phys.
Discussion started: 13 May 2019
© Author(s) 2019. CC BY 4.0 License.

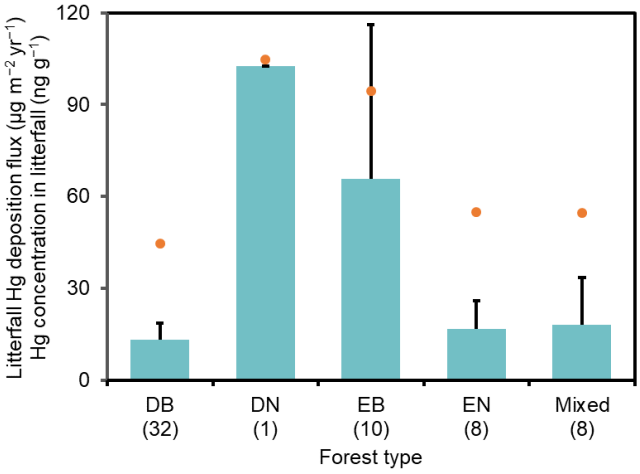

Figure 8. Litterfall Hg deposition fluxes (blue columns with black bars as standard deviations) and Hg concentrations in litterfall (orange dots) for different terrestrial surface types. The numbers in brackets stand for the numbers of samples. DB stands for deciduous broadleaf forests, DN stands for deciduous needle leaf forests, EB stands for evergreen broadleaf forests, and EN stands for evergreen needle leaf forests.